Qubit-oscillator systems in the ultrastrong-coupling regime and their potential for preparing nonclassical states

S. Ashhab[1,2] and Franco Nori[1,2]

[1] *Advanced Science Institute, The Institute of Physical and Chemical Research (RIKEN), Wako-shi, Saitama 351-0198, Japan*
[2] *Physics Department, Michigan Center for Theoretical Physics, The University of Michigan, Ann Arbor, Michigan 48109-1040, USA*

(Dated: April 20, 2010)

We consider a system composed of a two-level system (i.e. a qubit) and a harmonic oscillator in the ultrastrong-coupling regime, where the coupling strength is comparable to the qubit and oscillator energy scales. Special emphasis is placed on the possibility of preparing nonclassical states in this system. These nonclassical states include squeezed states, Schrödinger-cat states and entangled states. We start by comparing the predictions of a number of analytical methods that can be used to describe the system under different assumptions, thus analyzing the properties of the system in various parameter regimes. We then examine the ground state of the system and analyze its nonclassical properties. We finally discuss some questions related to the possible experimental observation of the nonclassical states and the effect of decoherence.

I. INTRODUCTION

The two-level system (or qubit) and the harmonic oscillator are the two most basic, and perhaps most often studied, components of physical systems. The paradigm of a qubit coupled to a harmonic oscillator has also been analyzed by numerous authors over the past few decades [1, 2]. Physical systems that can be described by this model include natural atoms coupled to optical or microwave cavities [2], superconducting qubits coupled to superconducting resonators [3–5], quantum dots or Cooper-pair boxes coupled to nanomechanical resonators [6–8], electrons interacting with phonons in a solid [9] and some models of chaotic systems [10].

In the early work on cavity quantum electrodynamics (QED) in atomic systems, the achievable atom-cavity coupling strengths were smaller than the atomic and cavity decay rates, usually limiting observations to only indirect signatures of the theoretically predicted phenomena. Recently, the strong-coupling regime, where the coupling strength is larger than the decay rates in the system, has been achieved [11]. In addition to atomic systems, the strong-coupling regime has been achieved in superconducting circuit-QED systems [3, 4], and superconducting-qubit-nanomechanical-resonator systems are approaching this regime [7]. In fact, superconducting systems are suited for achieving the so-called ultrastrong-coupling regime, where the qubit-oscillator coupling strength is comparable to the qubit and oscillator energy scales [12]. One can expect to find new phenomena in this regime that are not present in the weak or moderately strong coupling regimes. Indeed there have been a number of theoretical studies on this system analyzing some of its rich static and dynamical properties [13–18].

One reason why superconducting systems are well suited for the implementation of qubit-oscillator experiments is the flexibility they allow in terms of designing the different system parameters. For example, in the two earliest experiments on circuit QED, Chiorescu *et al.* [3] used a low-frequency oscillator, while Wallraff *et al.* [4] realized a resonant qubit-oscillator system. Subgigahertz qubits have also been realized in recent experiments [19], and there should be no difficulty in fabricating high-frequency oscillators. Therefore, all possible combinations of qubit and oscillator frequencies are accessible, in principle. One advantage of superconducting qubits over natural atoms is the additional control associated with the tunability of essentially all the qubit parameters [20], as will be discussed in more detail below. This tunability contrasts with the situation encountered with natural atoms, where the atomic parameters are essentially fixed by nature. This advantage can be seen clearly in the recent experiments where Fock states and arbitrary oscillator states were prepared in a superconducting qubit-oscillator system [21, 22]. We shall see, however, that the additional controllability comes at the price of having to deal with additional coupling channels to the environment, and this unwanted coupling can increase the fragility of nonclassical states.

In this paper we present analytical arguments and numerical calculations pertaining to the strongly coupled qubit-oscillator system from the point of view of the potential for preparing nonclassical states in this setup. These states include squeezed states or superpositions of macroscopically distinct states (i.e. Schrödinger-cat state) in the oscillator, as well as qubit-oscillator entangled states [23]. In this study, we shall consider all the different combinations of qubit and oscillator frequencies. We shall also analyze in some detail the effect of the tunability in the qubit parameters on the behaviour of the system.

The paper is organized as follows: In Sec. II we introduce the Hamiltonian that we shall use throughout the paper. In Sec. III we discuss various analytical methods that can be used to study the system under different assumptions, and we compare the predictions of these methods. In Sec. IV we present results of numerical calculations that demonstrate the properties of the energy eigenstates of the system, including the nonclassical

properties of the ground state. In Sec. V we discuss the possibility of preparing and detecting the three types of nonclassical states of interest. In Sec. VI we discuss the effect of decoherence on the robustness of nonclassical states. Section VII contains some concluding remarks.

II. HAMILTONIAN

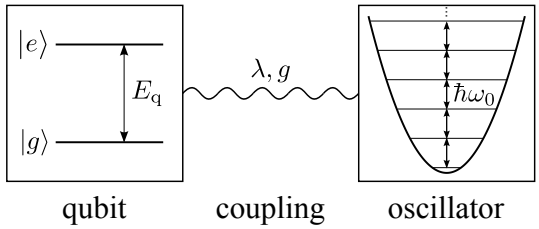

FIG. 1: Schematic diagram of the system under consideration. A qubit with energy separation $E_{\rm q}$ between its ground and excited states ($|g\rangle$ and $|e\rangle$) is coupled to a harmonic oscillator with characteristic frequency ω_0. The coupling strength is given by g or λ, depending on the language used to describe the oscillator.

The system that we consider here is a qubit coupled to a harmonic oscillator, as illustrated in Fig. 1. Rather than worry about deriving the model from a microscopic description of an electric circuit (see e.g. Refs. [12, 24, 25]), we shall assume that the description of the system as being composed of these two physical components with a coupling term of the standard form is an accurate description of the system.

The Hamiltonian of the system is given by:

$$\hat{H} = \hat{H}_{\rm q} + \hat{H}_{\rm ho} + \hat{H}_{\rm int}, \tag{1}$$

where

$$\begin{aligned} \hat{H}_{\rm q} &= -\frac{\Delta}{2}\hat{\sigma}_x - \frac{\epsilon}{2}\hat{\sigma}_z \\ \hat{H}_{\rm ho} &= \frac{\hat{p}^2}{2m} + \frac{1}{2}m\omega_0^2\hat{x}^2 \\ \hat{H}_{\rm int} &= g\hat{x}\hat{\sigma}_z, \end{aligned} \tag{2}$$

$\hat{\sigma}_x$ and $\hat{\sigma}_z$ are the usual Pauli matrices (with $\hat{\sigma}_z|\uparrow\rangle = |\uparrow\rangle, \hat{\sigma}_z|\downarrow\rangle = -|\downarrow\rangle$), and $\hat{x}$ and $\hat{p}$ are the position and momentum operators of the harmonic oscillator. The parameters Δ and ϵ are the gap and bias which characterize the qubit, m is the oscillator's effective mass, ω_0 is the oscillator's characteristic frequency, and g is the qubit-oscillator coupling strength. Note that in contrast to atomic cavity QED systems, where $\epsilon = 0$, this parameter is easily tunable in present-day experiments using superconducting qubits. We shall therefore treat ϵ as a tunable parameter (It is worth noting here that most past studies on the ultrastrong-coupling regime have focused on the case $\epsilon = 0$; however, see Ref. [17]). For definiteness, we shall take Δ and g to be positive.

It is convenient for some calculations to express the oscillator Hamiltonian using the creation ($\hat{a}^\dagger$) and annihilation ($\hat{a}$) operators:

$$\begin{aligned} \hat{a} &= \hat{X} + i\hat{P} \\ \hat{a}^\dagger &= \hat{X} - i\hat{P} \\ \hat{X} &= \sqrt{\frac{m\omega_0}{2\hbar}}\hat{x} \\ \hat{P} &= \frac{1}{\sqrt{2\hbar m\omega_0}}\hat{p}, \end{aligned} \tag{3}$$

which give

$$\begin{aligned} \hat{H}_{\rm ho} &= \hbar\omega_0\hat{a}^\dagger\hat{a} + \frac{1}{2}\hbar\omega_0 \\ \hat{H}_{\rm int} &= \lambda\left(\hat{a} + \hat{a}^\dagger\right)\hat{\sigma}_z \\ \lambda &= g\sqrt{\frac{\hbar}{2m\omega_0}}. \end{aligned} \tag{4}$$

The coupling strength can therefore be quantified either through g or λ.

We shall refer to the eigenstates of $\hat{H}_{\rm q}$ as the qubit's ground and excited states, denoted by $|g\rangle$ and $|e\rangle$, keeping in mind the caveat that this identification becomes less meaningful for strong qubit-oscillator coupling. The energies of these two states are $\pm E_{\rm q}/2$, where $E_{\rm q} = \sqrt{\Delta^2 + \epsilon^2}$. It is also useful to define an angle θ that characterizes the relative size of the $\hat{\sigma}_x$ and $\hat{\sigma}_z$ terms in the qubit Hamiltonian: $\tan\theta = \epsilon/\Delta$. The eigenstates of $\hat{H}_{\rm ho}$ are given by $|n\rangle$, where $n = 0, 1, 2, ...$, with energies given by $n\hbar\omega_0$ (up to the ground state energy $\hbar\omega_0/2$, which we ignore from now on). The integer n represents the number of excitations, to which we shall refer as photons, in the oscillator.

III. COMPARISON BETWEEN DIFFERENT ANALYTICAL METHODS

In this section we describe some analytical methods that can be used to determine the properties and behaviour of the system based on different assumptions (which are valid in different parameter regimes), and we compare the predictions of the different methods.

A. Weak coupling

The simplest limit is probably the weak-coupling limit [2], where $\lambda \ll E_{\rm q}, \hbar\omega_0$. Strictly speaking, one also needs to consider the number of photons in the oscillator when determining whether the weak-coupling condition is satisfied. However, since in this paper we focus on a system that remains close to its ground state, we assume a small number of photons in the oscillator. In the weak-coupling limit, one can think of the qubit and oscillator as being well-defined, separate physical systems

that interact weakly and can exchange excitations with one another [1].

In the limit of small λ, one can treat $\hat{H}_{\rm int}$ as a small perturbation in the total Hamiltonian. The energy eigenstates in the absence of this perturbation are given by $|n,g\rangle = |n\rangle \otimes |g\rangle$ and $|n,e\rangle = |n\rangle \otimes |e\rangle$, with energies $n\hbar\omega_0 \pm E_{\rm q}/2$ (recall that we ignore the $\hbar\omega_0/2$ term in the oscillator's energy).

When there are no degeneracies in the non-interacting system (i.e. in the Hamiltonian given by $\hat{H}_{\rm q} + \hat{H}_{\rm ho}$), the addition of the perturbation $\hat{H}_{\rm int}$ has only a small effect on the behaviour of the system. This perturbation only slightly modifies the energy levels and eigenstates of the Hamiltonian.

When $E_{\rm q} \approx \hbar\omega_0$, the states $|n,g\rangle$ and $|n-1,e\rangle$ are nearly degenerate (note that there is one such pair of nearly degenerate states for each value of n), and the perturbation term couples them. In particular, the relevant matrix elements are given by $\langle n,g|\,\hat{H}_{\rm int}\,|n-1,e\rangle = \lambda\sqrt{n}\cos\theta$, $\langle n,g|\,\hat{H}_{\rm int}\,|n,g\rangle = \langle n-1,e|\,\hat{H}_{\rm int}\,|n-1,e\rangle = 0$ and $\langle n-1,e|\,(\hat{H}_{\rm q} + \hat{H}_{\rm ho})\,|n-1,e\rangle - \langle n,g|\,(\hat{H}_{\rm q} + \hat{H}_{\rm ho})\,|n,g\rangle = E_{\rm q} - \hbar\omega_0$. In other words the effective Hamiltonian that one needs to consider is given by

$$\hat{H}_{\rm eff} = \begin{pmatrix} \delta/2 & \lambda\sqrt{n}\cos\theta \\ \lambda\sqrt{n}\cos\theta & -\delta/2 \end{pmatrix}, \qquad (5)$$

where $\delta = E_{\rm q} - \hbar\omega_0$. Using this Hamiltonian, one can analyze the behaviour of the system. In particular, when $E_{\rm q} = \hbar\omega_0$, an excitation oscillates back and forth between the qubit and oscillator with frequency $2\lambda\sqrt{n}\cos\theta$, which is commonly referred to as the Rabi frequency.

Degeneracies also occur when $E_{\rm q} = k\hbar\omega_0$, with k being any integer. In this case, one can go to higher orders in perturbation theory and obtain analytic, though sometimes cumbersome, expressions describing the properties and dynamics of the system. We shall not go any further in analyzing this situation here[26].

Note that the same results as those explained above (for the case $E_{\rm q} \approx \hbar\omega_0$) can be obtained by taking the term $\hat{H}_{\rm int}$ in the Hamiltonian and replacing it by its rotating-wave-approximation (RWA) form:

$$\hat{H}_{\rm int,RWA} = \lambda\cos\theta\left(\hat{a}\hat{\sigma}_+ + \hat{a}^\dagger\hat{\sigma}_-\right), \qquad (6)$$

where $\hat{\sigma}_\pm$ are the qubit raising and lowering operators ($\hat{\sigma}_+\,|g\rangle = |e\rangle$ etc.). This approximation therefore ignores the so-called counter-rotating terms in $\hat{H}_{\rm int}$, which are proportional to $\hat{a}^\dagger\hat{\sigma}_+$ and $\hat{a}\hat{\sigma}_-$, as well as a term proportional to $(\hat{a}+\hat{a}^\dagger)(|e\rangle\langle e| - |g\rangle\langle g|)$ that appears when $\epsilon \neq 0$. These terms would change the number of excitations in the system, thus mixing states that have a large energy separation (assuming $\lambda \ll E_{\rm q}, \hbar\omega_0$), and energy conservation suppresses such processes. The RWA therefore approximates the original Hamiltonian by one where the state $|n,g\rangle$ is coupled only to the state $|n-1,e\rangle$, which would lead to exactly the same algebra and results mentioned above. Some of the recent studies on ultrastrong coupling have analyzed the effects of the counter-rotating terms on the system dynamics [16, 18].

B. High-frequency, adiabatically adjusting oscillator

The next limit that we consider is that where the oscillator's characteristic frequency ω_0 is large compared to the qubit's energy splitting (i.e. $\hbar\omega_0 \gg E_{\rm q}$) and also compared to the coupling strength ($\hbar\omega_0 \gg \lambda$). In this case one can say that the oscillator remains in its initial energy eigenstate (i.e. ground state, first excited state, etc.), and this state follows adiabatically any changes in the qubit's state. This case was analyzed theoretically in Refs. [14, 15].

The procedure for adiabatically eliminating the high-frequency oscillator from the problem is straightforward. One starts by noting that the qubit is coupled to the oscillator through the operator $\hat{\sigma}_z$. As a result, one can think of the oscillator as always monitoring the qubit observable σ_z and adjusting to be in the instantaneous energy eigenstate that corresponds to that value of σ_z (Note here that if the qubit is in a superposition of two different σ_z states, each part of the superposition – with a well-defined value of σ_z – will have the oscillator in the corresponding energy eigenstate).

We therefore start by assuming that the qubit has a well-defined value of σ_z, equal to ± 1. The oscillator now feels the effective Hamiltonian (calculated from $\hat{H}_{\rm ho}$ and $\hat{H}_{\rm int}$):

$$\hat{H}_{\rm ho,eff}\Big|_{\sigma_z=\pm1} = \hbar\omega_0\hat{a}^\dagger\hat{a} \pm \lambda\left(\hat{a} + \hat{a}^\dagger\right). \qquad (7)$$

This Hamiltonian corresponds simply to the original oscillator Hamiltonian with a constant force term applied to it. This force term can be eliminated using the transformation

$$\hat{a}' = \hat{a} \pm \frac{\lambda}{\hbar\omega_0}, \qquad (8)$$

which gives

$$\hat{H}_{\rm ho,eff}\Big|_{\sigma_z=\pm1} = \hbar\omega_0\hat{a}'^\dagger\hat{a}' - \frac{\lambda^2}{\hbar\omega_0}. \qquad (9)$$

The above steps can also be carried out in the language of the operators $\hat{x}$ and $\hat{p}$:

$$\begin{aligned} \hat{H}_{\rm ho,eff}\Big|_{\sigma_z=\pm1} &= \frac{\hat{p}^2}{2m} + \frac{1}{2}m\omega_0^2\hat{x}^2 \pm g\hat{x} \\ x' &= x \pm \frac{g}{m\omega_0^2} \\ p' &= p \\ \hat{H}_{\rm ho,eff}\Big|_{\sigma_z=\pm1} &= \frac{\hat{p'}^2}{2m} + \frac{1}{2}m\omega_0^2\hat{x'}^2 - \frac{g^2}{2m\omega_0^2}. \end{aligned} \qquad (10)$$

The energy levels of the oscillator are given by $n\hbar\omega_0 - \lambda^2/(\hbar\omega_0)$, independently of the qubit's state. There will therefore not be a qubit-state-dependent energy that we need to take into account when we turn to analyzing the behaviour of the (slow) qubit. The oscillator's energy eigenstates, however, are slightly dependent on the state of the qubit. In particular,

$$\langle n_{\sigma_z=+1}|m_{\sigma_z=+1}\rangle = \langle n_{\sigma_z=-1}|m_{\sigma_z=-1}\rangle = \delta_{nm}, \quad (11)$$

and

$$\langle n_{\sigma_z=+1}|m_{\sigma_z=-1}\rangle = \begin{cases} e^{-2\lambda^2/(\hbar\omega_0)^2}\left(-\frac{2\lambda}{\hbar\omega_0}\right)^{m-n}\sqrt{\frac{n!}{m!}}L_n^{m-n}\left[\left(\frac{2\lambda}{\hbar\omega_0}\right)^2\right] & , \ m \geq n \\ e^{-2\lambda^2/(\hbar\omega_0)^2}\left(\frac{2\lambda}{\hbar\omega_0}\right)^{n-m}\sqrt{\frac{m!}{n!}}L_m^{n-m}\left[\left(\frac{2\lambda}{\hbar\omega_0}\right)^2\right] & , \ m < n, \end{cases} \quad (12)$$

where δ_{nm} is the Kronecker delta, and L_i^j are the associated Laguerre polynomials.

Having obtained the states of the high-frequency oscillator and the properties of these states, one can now turn to the slow part of the system, namely the qubit. We take any given value for the index n, which specifies the oscillator's state, and we use it to construct an effective qubit Hamiltonian for that value of n. Since there are two qubit states for each value of n, the effective Hamiltonian will be a 2×2 matrix operating in the space defined by the states $\left\{\left|\widetilde{n,\uparrow}\right\rangle, \left|\widetilde{n,\downarrow}\right\rangle\right\}$ (We use the tildes in order to emphasize that the oscillator's state is different from the state $|n\rangle$ of the free oscillator). The four relevant matrix elements can be calculated straightforwardly as

$$\begin{aligned} \left\langle\widetilde{n,\uparrow}\right| \hat{H}_{\rm q} \left|\widetilde{n,\uparrow}\right\rangle &= -\left\langle\widetilde{n,\downarrow}\right| \hat{H}_{\rm q} \left|\widetilde{n,\downarrow}\right\rangle = -\frac{\epsilon}{2} \\ \left\langle\widetilde{n,\uparrow}\right| \hat{H}_{\rm q} \left|\widetilde{n,\downarrow}\right\rangle &= \left\langle\widetilde{n,\downarrow}\right| \hat{H}_{\rm q} \left|\widetilde{n,\uparrow}\right\rangle \\ &= -\frac{\Delta}{2} e^{-2\lambda^2/(\hbar\omega_0)^2} L_n^0\left[\left(\frac{2\lambda}{\hbar\omega_0}\right)^2\right] \end{aligned} \quad (13)$$

The qubit is therefore described by the effective Hamiltonian

$$\hat{H}_{\rm eff} = -\frac{1}{2}\begin{pmatrix} \epsilon & \tilde{\Delta} \\ \tilde{\Delta} & -\epsilon \end{pmatrix}, \quad (14)$$

where $\tilde{\Delta}$ is given by Eq. (13) and can be thought of as the renormalized value of the gap Δ.

The exponential and Laguerre-function factors are both slightly smaller than one for small values of $\lambda/(\hbar\omega_0)$. The qubit therefore experiences a small reduction in the coupling (or 'tunnelling') between the states $|\uparrow\rangle$ and $|\downarrow\rangle$ in the weak-coupling limit ($\lambda \ll \hbar\omega_0$). This decrease in the renormalized value of Δ can be understood in terms of the qubit having to 'pull' the oscillator with it as it tunnels between the states $|\uparrow\rangle$ and $|\downarrow\rangle$, which would slow down the tunneling process. Note that the renormalized gap depends on the number of photons in the oscillator, which can lead to beating dynamics and other interesting phenomena that occur when several values of n are involved [14, 15].

If we keep increasing $\lambda/(\hbar\omega_0)$, without worrying about satisfying the condition $\lambda \ll \hbar\omega_0$, we find that the Laguerre polynomial and therefore the renormalized qubit gap vanish at n different $\lambda/(\hbar\omega_0)$ values (For example, for $n = 2$ there are two values of λ for which the renormalized gap vanishes). At these points, the states $\left|\widetilde{n,\uparrow}\right\rangle$ and $\left|\widetilde{n,\downarrow}\right\rangle$ are completely decoupled. Apart from this feature, the renormalized gap decreases as a Gaussian function with increasing $\lambda/(\hbar\omega_0)$. Note that while increasing λ there is no point that can be seen as a 'critical point' with a sudden change in behaviour. This situation contrasts with what happens in the two calculations that we shall discuss in the next two sections, and the meaning of the term critical point will become clearer there.

One might expect that the adiabatically-adjusting-oscillator approximation would break down when λ is comparable to, or larger than, $\hbar\omega_0$ (meaning that $\hbar\omega_0$ is not the largest energy scale in the Hamiltonian). The arguments in the previous paragraph might therefore seem of little significance. It turns out, however, that the results discussed above hold, even when $\lambda > \hbar\omega_0$. The reason why the approximation of an adiabatically adjusting oscillator is still valid in this case is that even though large changes in the oscillator's states can occur when the qubit's state changes, these large changes involve very slow processes that are governed by the renormalized gap. The oscillator can therefore adjust adiabatically to these slow processes. In other words, the condition that $\hbar\omega_0$ be the largest energy scale in the Hamiltonian is a sufficient but not necessary condition for the validity of the adiabatically-adjusting-oscillator approximation.

C. High-frequency, adiabatically adjusting qubit

We now take the limit where $E_{\rm q}$ is much larger than both $\hbar\omega_0$ and λ (Some analysis of this case was given in Ref. [15]). Similarly to what was done in Sec. III B, we

now say that the qubit remains in the same energy eigenstate (ground or excited state), and this state changes adiabatically following the dynamics of the slow oscillator. We therefore start by finding the energy eigenstates of the (fast-adjusting) qubit for a given state of the (slow) oscillator. Since the interaction between the qubit and the oscillator is mediated by the oscillator's position operator $\hat{x}$, we start the calculation by assuming that x has a well-defined value and treat the effective Hamiltonian (obtained from $\hat{H}_{\rm q}$ and $\hat{H}_{\rm int}$):

$$\hat{H}_{\rm q,eff}\Big|_x = -\frac{\Delta}{2}\hat{\sigma}_x - \frac{\epsilon}{2}\hat{\sigma}_z + gx\hat{\sigma}_z. \tag{15}$$

The eigenvalues and eigenstates of this Hamiltonian are given by:

$$\begin{aligned} E_{{\rm q},1|x} &= -\frac{1}{2}\sqrt{\Delta^2+(\epsilon-2gx)^2} \\ |g_x\rangle &= \cos\frac{\varphi}{2}|\uparrow\rangle + \sin\frac{\varphi}{2}|\downarrow\rangle \\ E_{{\rm q},2|x} &= \frac{1}{2}\sqrt{\Delta^2+(\epsilon-2gx)^2} \\ |e_x\rangle &= \sin\frac{\varphi}{2}|\uparrow\rangle - \cos\frac{\varphi}{2}|\downarrow\rangle \\ \tan\varphi &= \frac{\Delta}{\epsilon-2gx}. \end{aligned} \tag{16}$$

We can now take these results and use them to analyze the behaviour of the oscillator. We note here that since the variable x appears inside the square-root in the above expressions, the operators $\hat{x}$ and $\hat{p}$ lead to a more transparent analysis than the operators $\hat{a}$ and $\hat{a}^\dagger$. We therefore use the operators $\hat{x}$ and $\hat{p}$ for the remainder of this calculation.

Since the qubit's energy depends on the oscillator's position x, the oscillator's effective potential now acquires a new contribution (which depends on the qubit's state):

$$V_{\rm eff}(x) = \frac{1}{2}m\omega_0^2x^2 \pm \frac{1}{2}\sqrt{\Delta^2+(\epsilon-2gx)^2}. \tag{17}$$

The plus sign corresponds to the qubit being in the excited state, and the minus sign corresponds to the qubit being in the ground state. In addition to the above effect of the qubit on the oscillator, the qubit's state changes as the oscillator's position changes, and the oscillator's kinetic-energy term will also be modified in principle (this effect is similar to the renormalization of Δ encountered in Sec. III B). However, for a sufficiently high-frequency qubit, changes in the qubit's state will be small (see Appendix A), and consequently the change in the kinetic-energy term can be neglected.

We now note that the effective potential in Eq. (17) is no longer a harmonic potential. The second term describes one of the two branches of a hyperbola, depending on the qubit's state. It will therefore not be possible to derive general analytical results, and we have to start considering some special cases.

In the limit $E_{\rm q} \gg g|x|$ for the relevant values of x, the effective potential in Eq. (17) can be approximated by:

$$\begin{aligned} V_{\rm eff}(x) &\approx \frac{1}{2}m\omega_0^2x^2 \pm \left(\frac{\sqrt{\Delta^2+\epsilon^2}}{2} - \frac{\epsilon gx - g^2x^2}{\sqrt{\Delta^2+\epsilon^2}}\right) \\ &= \frac{1}{2}m\tilde{\omega}_0^2\left(x \mp \frac{\epsilon g}{m\tilde{\omega}_0^2E_{\rm q}}\right)^2 \pm \frac{E_{\rm q}}{2}, \end{aligned} \tag{18}$$

where

$$\tilde{\omega}_0^2 = \omega_0^2 \pm 2\frac{g^2}{mE_{\rm q}}. \tag{19}$$

The oscillator's effective potential is modified in two ways depending on the qubit's state. Firstly, the location of the minimum is shifted to the left or right by a distance proportional to $\epsilon/E_{\rm q} = \sin\theta$ (This effect is absent when the qubit is biased at the degeneracy point, where $\epsilon = 0$). Secondly, the oscillator's frequency is renormalized: According to Eq. (19), the oscillator's effective frequency is increased for the qubit's excited state and reduced for the qubit's ground state (This phenomenon is the basis of the so-called quantum-capacitance and quantum-inductance qubit-readout techniques [27]).

An interesting result appears when one considers the case where the qubit is in its ground state and

$$\frac{2g^2}{m\omega_0^2E_{\rm q}} > 1, \quad \text{i.e.} \quad \frac{4\lambda^2}{\hbar\omega_0E_{\rm q}} > 1. \tag{20}$$

In this case the renormalized frequency becomes imaginary. This result signals the presence of a critical point above which there is an instability in the system. In particular, our expansion of the square-root in Eq. (18) is no longer valid, the reason being that x would increase indefinitely under this approximation and the condition $E_{\rm q} \gg g|x|$ would be violated.

The instability obtained above would raise questions about the validity of the assumption of an adiabatically adjusting qubit above the critical point. Nevertheless, we shall not worry about this point now, and we continue the calculation. As a first step, we note that $V_{\rm eff}(x)$ in Eq. (17) is well behaved at $|x| \to \infty$. In particular,

$$V_{\rm eff}(x) = \frac{1}{2}m\omega_0^2x^2 \pm \left|gx - \frac{\epsilon}{2}\right| \quad \text{when} \quad |x| \gg \frac{\Delta}{g}, \frac{|\epsilon|}{g}. \tag{21}$$

We can therefore proceed with the calculation using the effective potential given in Eq. (17).

In order to make a few more statements about the case of strong coupling (i.e. above the critical point), it is useful to start with the case $\epsilon = 0$ and include a finite bias afterwards. When $\epsilon = 0$, the oscillator's effective potential takes the form

$$V_{\rm eff}(x) = \begin{cases} \left(\frac{1}{2}m\omega_0^2 \pm \frac{g^2}{\Delta}\right)x^2 \pm \frac{\Delta}{2} & , x \ll \Delta/g \\ \frac{1}{2}m\omega_0^2x^2 \pm |gx| & , x \gg \Delta/g \end{cases} \tag{22}$$

For the case with the qubit in its excited state (i.e. when one has the plus signs in the above expressions), the effective potential is a slightly non-harmonic potential, and one can expect the oscillator states to look more or less like the usual harmonic oscillator states. For the case with the qubit in its ground state, and when $2g^2/(m\omega_0^2\Delta) \ll 1$, one also has a slightly non-harmonic potential. For the qubit's ground state and $2g^2/(m\omega_0^2\Delta) > 1$ (which implies crossing the critical point), the oscillator's effective potential is a double-well potential. The locations of the minima can be obtained by setting $dV_{\rm eff}/dx = 0$ with $V_{\rm eff}$ given by Eq. (17): the minima are located at $\pm x_0$, with

$$x_0 = \sqrt{\frac{g^2}{m^2\omega_0^4} - \frac{\Delta^2}{4g^2}}. \tag{23}$$

If one goes well beyond the critical point, the above expression reduces to

$$x_0 \approx \frac{g}{m\omega_0^2}, \tag{24}$$

with minimum potential energy [measured relative to $V_{\rm eff}(0)$]

$$V_{\rm min} = V_{\rm eff}(\pm x_0) - V_{\rm eff}(0) \approx -\frac{g^2}{2m\omega_0^2}, \tag{25}$$

and curvature

$$\left.\frac{d^2V_{\rm eff}}{dx^2}\right|_{x=\pm x_0} \approx m\omega_0^2. \tag{26}$$

Note that this curvature is identical to that of the free oscillator (i.e. when $g = 0$).

One can use the above expressions to estimate the energy separation between the ground state and first excited state above the critical point. These two states will be the symmetric and antisymmetric superpositions of the ground states localized around the two minima in the double-well potential. The distance between the two minima is given by $2x_0$ from Eq. (24), and the height of the energy barrier separating the two minima is given by $-V_{\rm min}$ from Eq. (25). Using the Wentzel-Kramers-Brillouin (WKB) formula, one finds that the energy separation between the two lowest states (and also within similar pairs of higher energy levels) is exponential in the parameter $\sqrt{-mV_{\rm min}}x_0/\hbar$, which is proportional to $g^2/(m\omega_0^3\hbar)$, or alternatively $\lambda^2/(\hbar\omega_0)^2$. This scaling is the same as the one obtained in Sec. III B.

We now introduce ϵ to the problem. Far below the critical point, the effect of ϵ can be obtained easily from Eq. (18): the location of the minimum in the single-well effective potential is slightly shifted to the left or right. More care is required above the critical point, where one has the double-well effective potential. In this case, a finite value of ϵ breaks the symmetry between the left and right wells, thus giving an energetic preference for one of the two wells. In order to cause localization in the energy eigenstates, ϵ has to be larger than the energy separation within one of the energy-level pairs discussed above, i.e. ϵ needs to be larger than a quantity that is exponentially small in $g^2/(m\omega_0^3\hbar)$. Clearly, this localization happens at smaller values of ϵ as one goes deeper into the bistability region. This result means that the superpositions involving both wells become increasingly fragile with increasing coupling strength.

Finally we note that above the critical point, one finds that the condition $E_{\rm q} \gg g|x|$ can no longer be satisfied for any of the energy eigenstates. Therefore, one might expect that the present approximation cannot be trusted. As we discussed in Sec. III B, however, the above results hold even when $\lambda > E_{\rm q}$. In that case the energy eigenstates are either localized close to one of the local minima or involve very slow tunneling between the two wells of the effective double-well potential. The qubit can adjust adiabatically to such slow tunneling processes. It is worth mentioning here that when λ is the largest energy scale in the Hamiltonian, the approximations of this section and Sec. III B are both valid, and either one of the two approaches can be used to answer any given question.

D. Semiclassical calculation

A semiclassical calculation can go as follows (alternative semiclassical calculations can be found in [10, 13, 15]): The five different variables x, p, σ_x, σ_y and σ_z are treated as classical variables whose dynamics obeys the Hamiltonian in Eqs. (1) and (2), without the hats. These variables obey the constraint $C = \sigma_x^2 + \sigma_y^2 + \sigma_z^2 = 1$. One can therefore find the ground state relatively easily by minimizing the Hamiltonian under the above constraint. Minimizing the function $\tilde{H} = H - \mu C$, with μ being a Lagrange multiplier, results in the set of equations

$$\begin{aligned}
\frac{d\tilde{H}}{dx} &= m\omega_0^2 x + g\sigma_z = 0 \\
\frac{d\tilde{H}}{dp} &= \frac{p}{m} = 0 \\
\frac{d\tilde{H}}{d\sigma_x} &= -\frac{\Delta}{2} - 2\mu\sigma_x = 0 \\
\frac{d\tilde{H}}{d\sigma_y} &= -2\mu\sigma_y = 0 \\
\frac{d\tilde{H}}{d\sigma_z} &= -\frac{\epsilon}{2} + gx - 2\mu\sigma_z = 0,
\end{aligned} \tag{27}$$

which are to be solved under the constraint $\sigma_x^2+\sigma_y^2+\sigma_z^2 = 1$. The first four equations lead to $x = -g\sigma_z/(m\omega_0^2)$, $p = 0$, $\mu = -\Delta/(4\sigma_x)$, and $\sigma_y = 0$. The constraint gives $\sigma_x = \pm\sqrt{1-\sigma_z^2}$. One is therefore left with the equation

$$-\frac{\epsilon}{2} - \frac{g^2\sigma_z}{m\omega_0^2} \pm \frac{\Delta\sigma_z}{2\sqrt{1-\sigma_z^2}} = 0, \tag{28}$$

which can be re-expressed as

$$-\frac{\epsilon}{\Delta}-\left(\frac{2g^2}{m\omega_0^2\Delta}\pm\frac{1}{\sqrt{1-\sigma_z^2}}\right)\sigma_z=0. \qquad (29)$$

The above equation cannot be solved in closed form, in general. However, one can make some general statements about the solution (see Fig. 2). For the plus sign (Fig. 2a), the second term in Eq. (29) is a monotonically decreasing function that approaches $+\infty$ when $\sigma_z \to -1$ and approaches $-\infty$ when $\sigma_z \to 1$. There is therefore one solution to the equation in that case. It turns out that this solution does not correspond to the ground state (This fact can be seen as simply a result of comparing the energies of the different solutions). The ground state is obtained when using the minus sign. In this case, there are three possibilities: The first possibility is to have $2g^2 < m\omega_0^2\Delta$. In this case (Fig. 2c), we find that the second term in Eq. (29) is a monotonically increasing function that approaches $-\infty$ when $\sigma_z \to -1$ and approaches $+\infty$ when $\sigma_z \to 1$. There is therefore only one solution to Eq. (29). The second and third possibilities for the solutions of Eq. (29) occur when $2g^2 > m\omega_0^2\Delta$. In this case (Figs. 2e and 2g), the second term in Eq. (29) develops a local maximum and a local minimum between $\sigma_z = -1$ and $\sigma_z = 1$. Depending on the value of ϵ, there can be either one or three solutions. In particular, when $\epsilon = 0$, the three solutions are given by $\sigma_z = 0$, which turns out to be an unstable stationary point, and $\sigma_z = \pm\sqrt{1-(m\omega_0^2\Delta/2g^2)^2}$, which are two degenerate ground states (It is easy to verify that this result agrees with Eq. 23).

One can intuitively understand the effect of having a finite value of ϵ using the language of Sec. III C. For $\epsilon = 0$, one has an effective trapping potential for the variable x, and this potential has the shape of a harmonic-oscillator-like single-well potential when $2g^2 < m\omega_0^2\Delta$ and a double-well potential when $2g^2 > m\omega_0^2\Delta$. This situation explains the existence of one ground state when $2g^2 < m\omega_0^2\Delta$ and two degenerate ground states when $2g^2 > m\omega_0^2\Delta$. The effect of adding ϵ to the problem is to create a tilt in the effective trapping potential; a positive value of ϵ favours the negative-x solution (here we have in mind the ground-state solution). If the tilt is weak, one has a global minimum in the deeper well and a local minimum in the shallower well. If the tilt exceeds a certain critical value, the shallow well is eliminated, and one recovers a single-well potential.

We make a final note on the fact that we started the calculation by raising a question related to the ground state but found multiple solutions. The reason for this result is the fact that Eq. (27) locates all stationary points, and not only the ground state. The calculation therefore identifies both the ground state and also high-energy stationary points that are either dynamically unstable or dynamically stable but can still relax to lower-energy states.

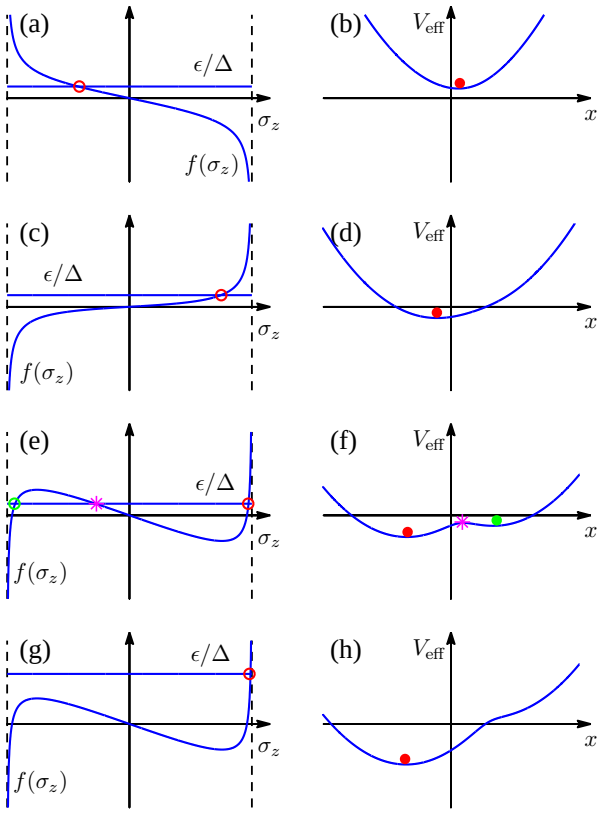

FIG. 2: (Color online) Graphical solution of Eq. (29) (left) and the associated effective potentials from Sec. III C (right) in the different possible cases. The horizontal lines in the left panels represent the first term in Eq. (29), and the function $f(\sigma_z)$ is the second term in the equation. The circles mark the stable solutions of Eq. (29), and the dots in the right panels mark the minima in the effective potential of Sec. III C, i.e. Eq. (17). The magenta stars in panels (e) and (f) mark an unstable stationary point, i.e. a local maximum in the effective potential. Panels (a) and (b) correspond to the plus signs in Eqs. (17) and (29), and panels (c-h) correspond to the minus signs. In panels (c) and (d), the coupling is below the critical point, i.e. $2g^2 < m\omega_0^2 E_{\rm q}$. In panels (e) and (f), the coupling is above the critical point and ϵ is small. In panels (g) and (h), the coupling is above the critical point and ϵ is large.

E. Concluding remarks

We conclude this section with some remarks on the conceptual ideas and predictions of the different analytical methods. The standard perturbation-theory procedure is well suited for the weak-coupling limit. One can use it to systematically obtain accurate approximations for the energy eigenstates and dynamics of the system. The two approximations involving one subsystem, either the qubit or the oscillator, adjusting adiabatically to the slow dynamics of the other one are based on the conceptual picture of the separation between different time scales in the problem. As formulated above, they involve only one level of approximation, in contrast to

the order-by-order expansion involved in perturbation theory. The time-scale-separation-based approximations can, however, be constructed formally as the lowest-order approximation in a systematic procedure sometimes referred to as adiabatic elimination of fast variables [28] or Van Vleck perturbation theory [29]. The semiclassical calculation treats the dynamical variables classically and is at first sight not related to any specific approximation related to the system parameters.

The weak-coupling approximation is suited for studying the excitation-exchange dynamics between the qubit and oscillator, but it does not give any hint of an instability in the system. The main result of the adiabatically-adjusting-oscillator approximation is the renormalized qubit gap. Apart from the oscillatory behaviour in the gap, the Gaussian-function decrease at large $\lambda/(\hbar\omega_0)$ values is a signature of the strong entanglement between the qubit and the oscillator in the energy eigenstates. Nevertheless, no 'critical point', i.e. a point that is associated with a sudden change in any of the effective qubit parameters (particularly the renormalized gap), is obtained in that calculation. The adiabatically-adjusting-qubit approximation predicts a reduced effective oscillator frequency for weak coupling (and assuming that the qubit is in its ground state), and a qualitative change in behaviour upon crossing the critical point

$$\frac{4\lambda^2}{\hbar\omega_0 E_{\mathrm{q}}} = 1. \tag{30}$$

Above the critical point, the energy eigenstates can be highly entangled qubit-oscillator states. As in the adiabatically-adjusting-oscillator approximation, the separation between neighbouring energy levels is found to follow a Gaussian-function dependence in the parameter $\lambda/(\hbar\omega_0)$. The adiabatically-adjusting-oscillator and adiabatically-adjusting-qubit approximations give different predictions regarding the typical value of λ at which the Gaussian-function decrease in energy separation starts: the former gives $\lambda \sim \hbar\omega_0$ and the latter gives $\lambda \sim \sqrt{\hbar\omega_0\Delta}$. The semiclassical calculation produces the same critical-point condition as the adiabatically-adjusting-qubit approximation. Even though the semiclassical calculation naturally cannot produce any entangled-state solutions, its results can be used as a starting point for studying quantum superpositions of the different semiclassical solutions.

One could understand the reason for the absence of a critical point in the case of a high-frequency oscillator as having to do with the pairing of energy levels. In this case, the energy levels form pairs all the way from $\lambda = 0$ to $\lambda \to \infty$. In contrast, in the case of a high-frequency qubit the low-lying levels are equally spaced for small values of λ. As λ increases, the energy levels start approaching each other while remaining equally spaced, a situation that corresponds to a decreasing renormalized oscillator frequency. At the point where the energy levels are expected to collapse to a single, highly degenerate energy level, they pair up and the different pairs start moving away from each other. The energy levels now resemble those of an increasingly deep double-well potential. Thus the energy levels and energy eigenstates exhibit two qualitatively different structures below and above the critical point.

It is worth mentioning that the adiabatically-adjusting-oscillator and adiabatically-adjusting-qubit approximations start with similar, or symmetric, reasoning. The asymmetry in the results is mainly due to the different dependence in the energy levels and energy eigenstates of the fast subsystem on the state of the slow subsystem. In the case of a fast qubit, the qubit's energy produces the largest effect on the slow oscillator. In the case of a fast oscillator, the oscillator's energy does not depend on the state of the qubit, and only the changes in the energy eigenstates lead to effective changes to the behaviour of the slow qubit.

One might wonder why the results of the semiclassical calculation agree with those of the high-frequency-qubit approximation. This agreement can be understood by noting first that the oscillator has continuous variables, such that it is conceivable that certain states will be described to a good approximation using classical variables (In this context one can think of coherent states, which to a good approximation behave classically). When the qubit's frequency is high, it is also conceivable that the qubit's state, which for example follows the instantaneous ground state, can be described by the classical variables that specify the instantaneous ground state. In this case, one can expect the semiclassical calculation to give good results. One can also use this argument to conclude that a phase-transition-like singularity will occur in the limit $\hbar\omega_0/E_{\mathrm{q}} \to 0$, where the semiclassical calculation can be expected to give exact results. In contrast, in the limit of a low-frequency qubit, the dynamics will necessarily be described by the coupling of two discrete quantum states, and this situation cannot be described well using a semiclassical approximation.

In the context of discussing the phase-transition-like bifurcation in this system, it is worth mentioning a related system with a true phase transition: the Dicke model [30]. If one replaces the single qubit by a large number of qubits with equal values of E_{q}, all coupled to the same cavity with the same value of λ, then by taking the appropriate thermodynamic limit ($N \to \infty$, $\lambda^2 N = \tilde{\lambda}^2$) one finds a phase transition between states similar to those discussed above [31]. The critical point is given by the condition $4\tilde{\lambda}^2 = \hbar\omega_0 E_{\mathrm{q}}$, in analogy to the critical-point condition discussed in Secs. III C and III D. In contrast to the single-qubit case, however, the phase transition now occurs regardless of the relation between the qubit and oscillator frequencies. Note that the qubits behave collectively as a single large spin in this case (and for low-lying states a large spin behaves similarly to a harmonic oscillator), such that the entire system can be approximated by two coupled oscillators. Note also that the semiclassical calculation arises naturally in this case: when the effective spin has an infinite number of allowed

states, it is natural to make a classical approximation where fluctuations in the spin are small compared to the total size of the available state space.

IV. NUMERICAL CALCULATIONS

In this section we present results of numerical calculations that demonstrate the properties of the system in the different parameter regimes. In particular, we perform calculations for the resonant case, the high-frequency-oscillator case and the high-frequency-qubit case. We also vary the qubit bias ϵ, or alternatively the angle θ, in order to analyze its effect on the properties of the system.

A. Energy-level spectrum

In Fig. 3 we plot the energies of the lowest ten levels as a function of the coupling strength λ in the resonant case $\hbar\omega_0 = E_{\rm q}$. When $\epsilon = \lambda = 0$, the ground state is non-degenerate and each higher energy level is doubly degenerate. The separation between the levels is $\hbar\omega_0$, which is also equal to $E_{\rm q}$. As λ increases, the energy levels shift up or down, and several avoided crossings are encountered. In the large λ limit, all energy levels become doubly degenerate (i.e. they form pairs), including the ground state. The separation between the different pairs of energy levels in this limit is again $\hbar\omega_0$. These results agree with the picture of the effective double-well potential of Sec. III C. For a small but finite bias ϵ (i.e. small but finite θ) and small coupling strength λ, the overall energy level structure is similar to that in the $\epsilon = 0$ case, except that the levels do not approach each other as much at the avoided crossings. In the large λ limit, there are no degeneracies: the energy levels are separated by the alternate distances ϵ and $\hbar\omega_0 - \epsilon$. This structure reflects the small asymmetry in the double-well potential caused by a small tilt. For large θ (i.e. $\sin\theta \sim 1$), all features in the spectrum are suppressed, except for the overall decrease in the energy with increasing λ.

In order to examine the strong-coupling limit more closely, in Fig. 4 we plot the energy-level separation between the lowest two energy levels. The results agree with the predictions of Eq. (13): deep in the strong-coupling regime, the separation within the pairs of energy levels is given by $E_{2n+2} - E_{2n+1} \sim (\lambda/\hbar\omega_0)^n \exp\{-2(\lambda/\hbar\omega_0)^2\}$ for $\epsilon = 0$ and by ϵ for $\epsilon \neq 0$.

In Fig. 5 we plot the energies of the lowest ten levels as a function of λ in the case of a high-frequency oscillator, i.e. when $E_{\rm q} \ll \hbar\omega_0$. As explained in Sec. III B, if one considers a pair of energy levels, e.g. the lowest two energy levels, one has a modified effective qubit Hamiltonian. When $\lambda = 0$, one recovers the bare qubit Hamiltonian. As λ increases, the effective qubit gap Δ decreases and approaches zero in the limit $\lambda/(\hbar\omega_0) \to \infty$. In Fig. 6 we plot the separations within the four lowest pairs of energy levels. The effective gap follows the shape of a

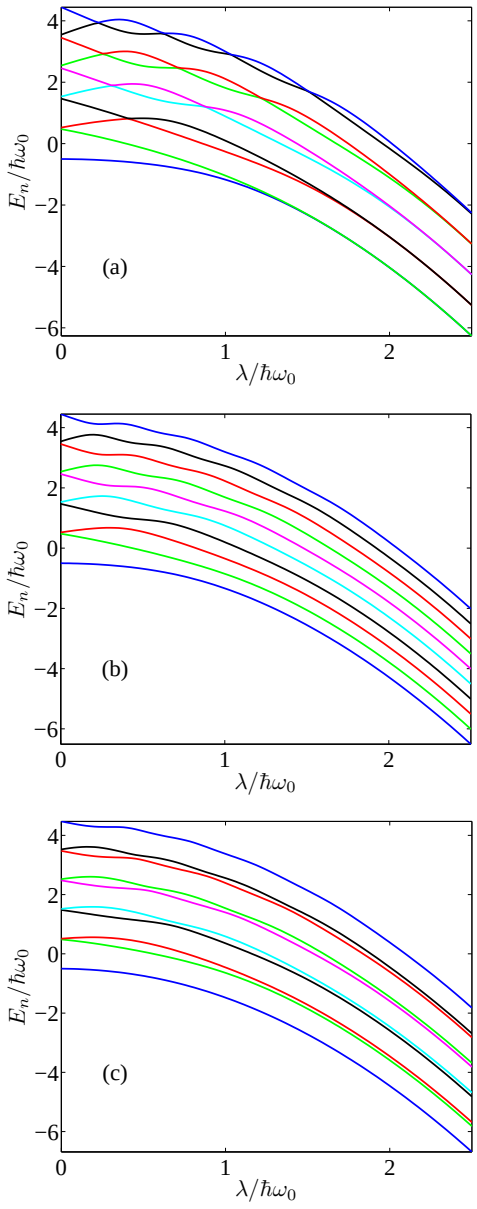

FIG. 3: (Color online) Lowest ten energy levels in the resonant case, i.e. when $\hbar\omega_0/E_{\rm q} = 1$. The rescaled energy $E_n/(\hbar\omega_0)$ with $n = 1, 2, ..., 10$ is plotted as a function of the rescaled coupling strength $\lambda/(\hbar\omega_0)$. Panels (a), (b) and (c) correspond to $\theta = 0, \pi/6$ and $\pi/3$, respectively [recall that $\theta = \arctan(\epsilon/\Delta)$].

Gaussian function times a Laguerre polynomial, vanishing at the zeros of the Laguerre polynomial. As θ is increased from zero, i.e. as the ratio Δ/ϵ decreases, the dependence of the energy-level separation on the coupling strength becomes weaker (This phenomenon can be seen by comparing the different panels in Fig. 6). Note that the location of the peaks does not change, but the effect of the gap on the energy levels becomes smaller with increasing θ.

In Fig. 7 we plot the energies of the lowest ten levels as a function of λ in the case of a high-frequency qubit,

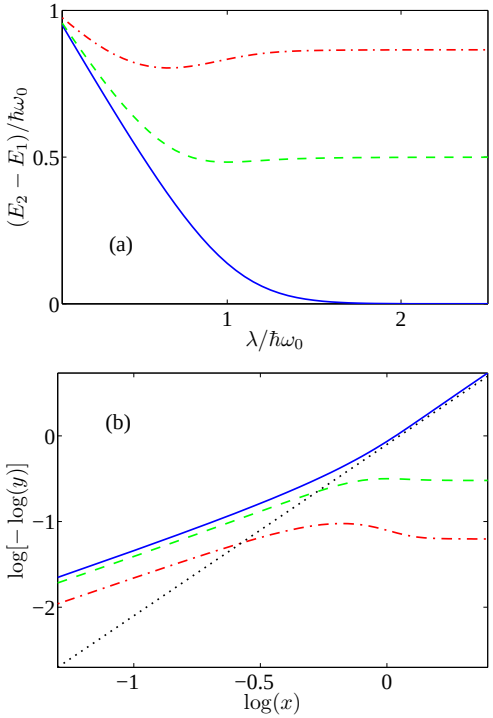

FIG. 4: (Color online) The separation between the lowest two energy levels in the resonant case, i.e. when $\hbar\omega_0/E_\mathrm{q} = 1$. In (a), the rescaled energy separation $(E_2 - E_1)/(\hbar\omega_0)$ is plotted as a function of the rescaled coupling strength $\lambda/(\hbar\omega_0)$. The blue, solid line corresponds to $\theta = 0$; the green, dashed line corresponds to $\theta = \pi/6$; and the red, dash-dotted line corresponds to $\theta = \pi/3$. In (b), the same data is plotted on a logarithmic scale in order to make a comparison with the formula $E_2 - E_1 = \Delta \exp\{-2(\lambda/\hbar\omega_0)^2\}$ from Eq. (13): x and y in the axis labels refer to the axis labels in (a). The black, dotted line shows the asymptotic behavior of the above formula. The good fit between the blue and black lines means that the numerical results agree with the results of Sec. III (We could extend the range of agreement by plotting $\log[\log(\Delta/\hbar\omega_0) - \log(y)]$; however, we are mostly interested in demonstrating the agreement for large values of x, where this modification would have little effect on the shape of the blue curve). Similar figures can be generated for the other values of $\hbar\omega_0/E_\mathrm{q}$. However, we do not show such figures here.

i.e. when $E_\mathrm{q} \gg \hbar\omega_0$. The most dramatic effects occur for $\theta = 0$. The ground-state energy remains essentially constant between $\lambda = 0$ and $\lambda = \sqrt{\hbar\omega_0\Delta}/2$. Beyond this point the ground-state energy decreases indefinitely with increasing λ. Furthermore, below the critical point, the low-lying energy levels approach each other with increasing λ as if they were going to collapse to one point, as would be expected for a vanishing $\tilde{\omega}_0$. Above the critical point, the energy levels form pairs whose intra-pair separation decreases with increasing λ. The above scenario is suppressed as θ is increased. There is no longer any sign of a critical point, and the energy-level separations are independent of λ.

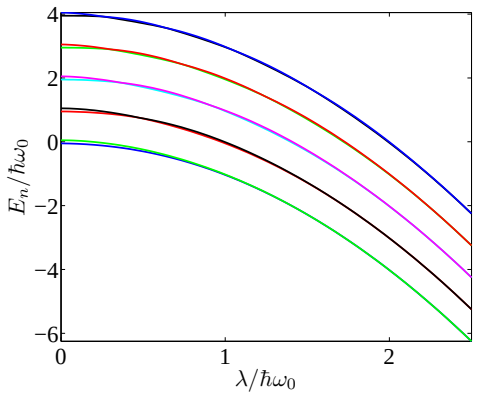

FIG. 5: (Color online) Lowest ten energy levels in the case of a high-frequency oscillator; $\hbar\omega_0/E_\mathrm{q} = 10$. Here we only show the results for $\theta = 0$, because the overall appearance of the plots is independent of θ. More details can be seen in Fig. 6.

B. Squeezing, entanglement, and 'cat-ness' in the ground state

One obvious possibility for the preparation of squeezed, entangled or Schrödinger-cat states in the case of ultrastrong coupling is to have a ground state that exhibits one of these unusual properties. With this point in mind, in this section we analyze the oscillator's squeezing and cat-ness as well as the qubit-oscillator entanglement in the ground state for different choices of system parameters.

As a first step, we plot the Q function and the Wigner function of the oscillator's state in the ground state of the coupled system. The Q function is given by

$$Q(X,P) = \frac{1}{\pi}\left\langle X+iP\right|\rho_\mathrm{osc}\left|X+iP\right\rangle, \qquad (31)$$

where ρ_osc is the oscillator's reduced density matrix after tracing out the qubit from the ground state, $\rho_\mathrm{osc} = \mathrm{Tr}_\mathrm{q}\{|\Psi_\mathrm{GS}\rangle\langle\Psi_\mathrm{GS}|\}$ with $|\Psi_\mathrm{GS}\rangle$ being the ground state of the combined system, and the bra and ket in the above formula are coherent states:

$$|\alpha\rangle = \exp\{\alpha\hat{a}^\dagger - \alpha^*\hat{a}\}\,|0\rangle\,. \qquad (32)$$

The state $|0\rangle$ represents the vacuum state with the oscillator in its ground state. The Wigner function is given by

$$W(X,P) = \frac{1}{2\pi\hbar}\int_{-\infty}^{\infty}\left\langle X+\frac{1}{2}X'\right|\rho_\mathrm{osc}\left|X-\frac{1}{2}X'\right\rangle e^{iPX'}dX', \qquad (33)$$

where the bra and ket are now eigenstates of the position operator $\hat{x}$, i.e. they are highly localized in configuration space. The Q and Wigner functions for a sequence of λ values are shown in Fig. 8.

Going beyond the pictorial description shown above, a quantifier for both the squeezing and cat-ness of the oscillator's state is the set of two squeezing parameters

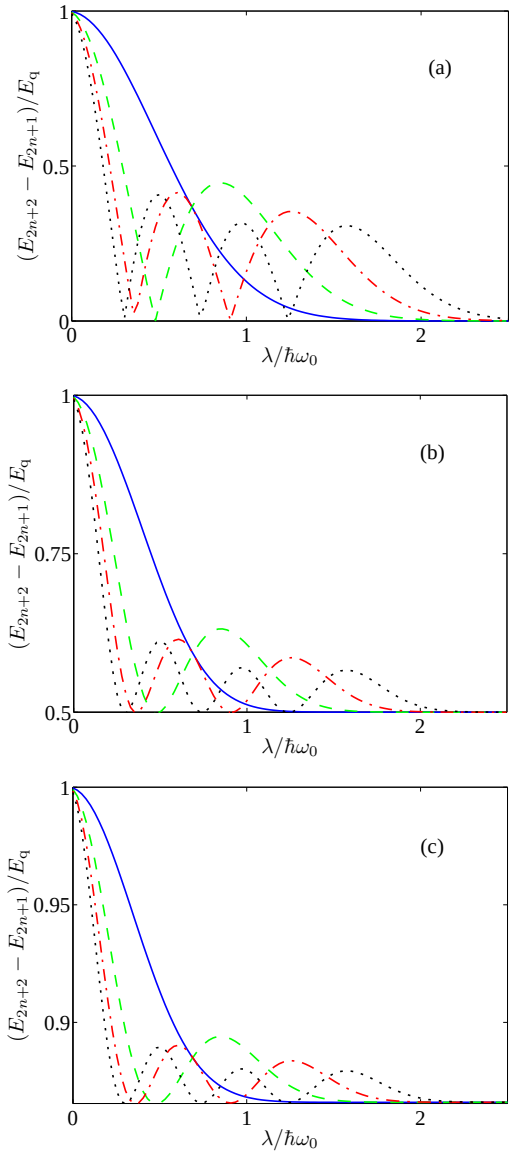

FIG. 6: (Color online) The rescaled energy separation $(E_{2n+2} - E_{2n+1})/E_q$ within the lowest four pairs of energy levels [i.e. for $n = 0$ (blue, solid line), 1 (green, dashed line), 2 (red, dash-dotted line) and 3 (black, dotted line)], as a function of $\lambda/(\hbar\omega_0)$. As in Fig. 5, we take $\hbar\omega_0/E_q = 10$. In panels (a), (b) and (c), $\theta = 0, \pi/6$ and $\pi/3$, respectively. Note that the minimum value on the y-axis is given by $\sin\theta$ and is different in the three panels.

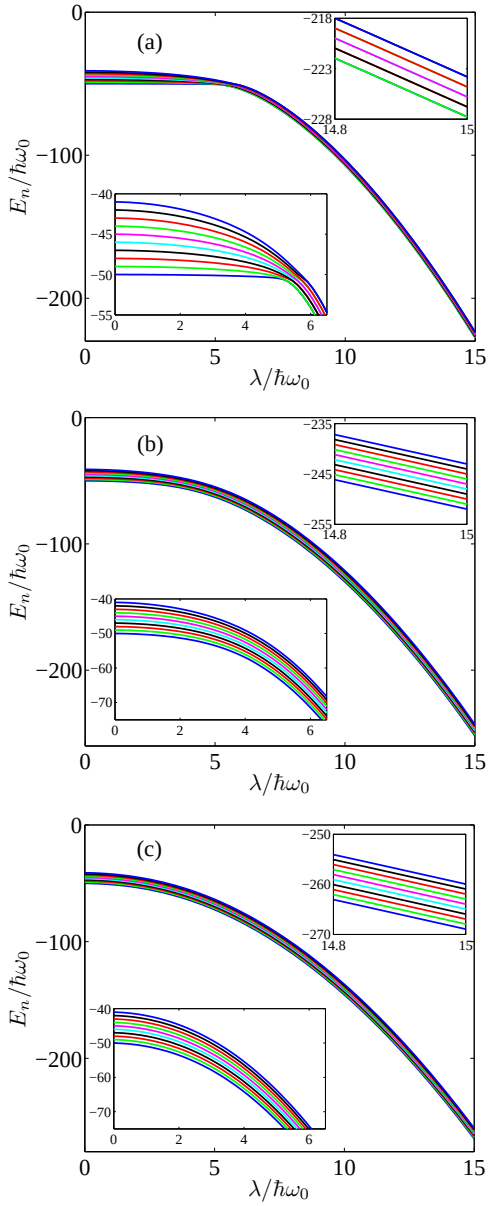

FIG. 7: (Color online) Lowest ten energy levels in the case of a high-frequency qubit; $\hbar\omega_0/E_q = 0.01$. In panels (a), (b) and (c), $\theta = 0, \pi/6$ and $\pi/3$, respectively. The insets show enlarged views of the weak-coupling and strong-coupling regions.

in the x and p quadratures as well as the product of the quadrature variances (Note here that the oscillator's state is always mirror-symmetric with respect to the x axis in the setup under consideration, giving $\langle\hat{p}\rangle = 0$). After the appropriate conversion into dimensionless variables, these quantifiers are given by

$$s_x = 4\left\langle\left(\hat{X} - \langle\hat{X}\rangle\right)^2\right\rangle - 1$$

$$s_p = 4\left\langle\left(\hat{P} - \langle\hat{P}\rangle\right)^2\right\rangle - 1$$

$$K = \left\langle(\hat{x} - \langle\hat{x}\rangle)^2\right\rangle\left\langle(\hat{p} - \langle\hat{p}\rangle)^2\right\rangle = \frac{\hbar^2}{4}(1 + s_x)(1 + s_p). \quad (34)$$

The parameter K is equal to $\hbar^2/4$ for a minimum-uncertainty state (including both coherent and quadrature-squeezed states) and is larger than that lower bound for any other state (including Schrödinger-

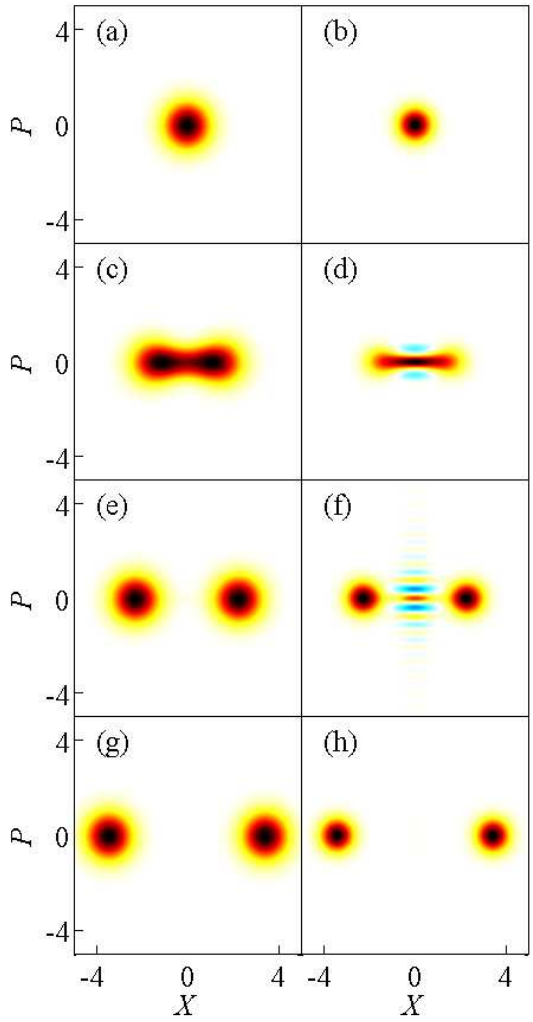

FIG. 8: (Color online) The Q function (left) and the Wigner function (right) of the oscillator's state in the ground state of the combined system. Here we take $\hbar\omega_0/\Delta = 0.1$ and $\epsilon = 0$. The different panels correspond to $\lambda/(\hbar\omega_0) = 0.5$ (a,b), 2 (c,d), 2.5 (e,f) and 3.5 (g,h). For clarity, we adjust the color scheme in the different panels such that the highest point is always black. The red and yellow colors also correspond to positive values. The white color corresponds to zero value. The blue color represents negative values of the Wigner function. The oscillator's state goes from a coherent state with no photons (i.e. the vacuum state) in the absence of coupling, to a squeezed state for low to moderate coupling strengths and then to a qubit-oscillator entangled state for very strong coupling. Note that the state in panels g and h is highly nonclassical, in particular highly entangled, even though this fact cannot be seen in the Q and Wigner functions.

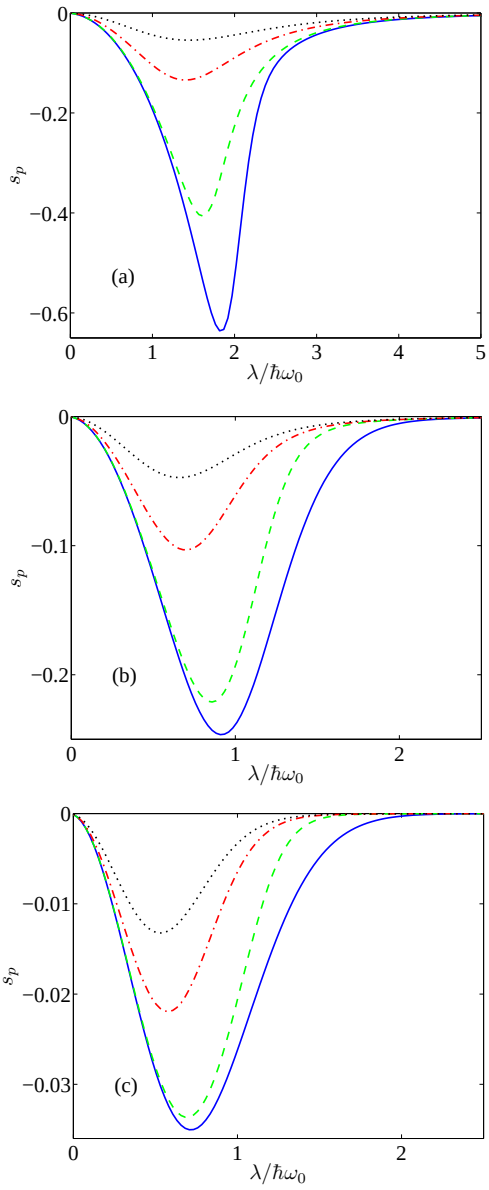

FIG. 9: (Color online) The momentum squeezing parameter s_p as a function of $\lambda/(\hbar\omega_0)$ for $\hbar\omega_0/\Delta = 0.1$ (a), 1 (b) and 10 (c). The different curves correspond to $\epsilon/\Delta = 0$ (blue, solid line), 0.1 (green, dashed line), 0.5 (red, dash-dotted line) and 1 (black, dotted line). The oscillator's state becomes squeezed as the coupling strength λ increases, but then it reaches a maximum and goes back to zero as the qubit and oscillator get entangled in the strong-coupling regime. Note that the maximum achievable squeezing decreases with increasing $\hbar\omega_0/\Delta$.

cat and qubit-oscillator entangled states). In Fig. 9 we plot the momentum squeezing parameter as a function of the coupling strength λ. For small values of λ, the squeezing increases with increasing λ. However, as λ increases further and the ground state becomes more and more entangled, the squeezing is lost. The maximum achievable squeezing is largest for the case of a high-frequency qubit, $\hbar\omega_0 \ll \Delta$. Indeed, as explained in Sec. III C, the oscillator's effective potential becomes

flatter and flatter as one approaches the critical point, leading to a momentum squeezing parameter close to -1.

As $|s_p|$ increases, one can ask whether the oscillator's state is a quadrature-squeezed, minimum-uncertainty state or it deviates from this ideal squeezed state. The answer to this question can be obtained by analyzing the parameter K. We do not show any plots of this parameter here. The main results are as follows: For the case $\epsilon = 0$, K increases slowly and remains close to $\hbar^2/4$ as s_p increases, but near the maximum squeezing point, K starts increasing rapidly and diverges for $\lambda/(\hbar\omega_0) \to \infty$. For finite values of ϵ, K increases slightly above $\hbar^2/4$, but then turns and goes back to $\hbar^2/4$ as s_p goes back to zero in the strong-coupling limit.

We have seen that squeezed states are obtained for weak to moderate coupling. The question now is what states we have for strong coupling. The Q functions and the s_p and K results discussed above do not distinguish between a Schrödinger-cat state in the oscillator and a qubit-oscillator entangled state. The Wigner function has negative values for moderately strong coupling (Figs. 8d and 8f), indicating nonclassical states of the Schrödinger-cat type (Note that quadrature-squeezed states have nonnegative Wigner functions). In order to distinguish more clearly between Schrödinger-cat states in the oscillator and qubit-oscillator entangled states, we now analyze the entanglement properties in the ground state.

The entanglement is quantified by the entropy S of the qubit's state. This quantity is obtained by calculating the ground state of the combined system $|\Psi_{\rm GS}\rangle$, using it to obtain the qubit's reduced density matrix in the ground state $\rho_{\rm q} = {\rm Tr}_{\rm osc}\{|\Psi_{\rm GS}\rangle\langle\Psi_{\rm GS}|\}$, and then evaluating the entropy of that state $S = -{\rm Tr}\{\rho_{\rm q}\log_2\rho_{\rm q}\}$.

In Fig. 10 we plot the qubit's ground-state entropy as a function of λ. For $\epsilon = 0$ the entropy increases from zero to one as λ increases from zero to values much larger than all other parameters in the problem. Demonstrating the fragility of the entangled states in the large-λ limit, Fig. 10 shows that the entanglement drops rapidly (especially for large values of λ) when ϵ is increased.

By comparing Figs. 9 and 10, we can see that the rise in the qubit-oscillator entanglement is correlated with the reversal of the squeezing. One therefore goes from a squeezed state in the oscillator to a qubit-oscillator entangled state. We do not find any set of parameters where the ground state contains an unentangled Schrödinger-cat state in the oscillator.

The numerical results show that the case $\hbar\omega_0 \ll E_{\rm q}$ is most suited for the preparation of squeezed states, as can be seen by comparing the maximum achievable squeezing in the different parameter regimes. The opposite case ($\hbar\omega_0 \gg E_{\rm q}$) is most suited for the preparation of entangled states, as seen from the extreme fragility of these states for the case $\hbar\omega_0 \ll E_{\rm q}$. In fact, all the nonclassical properties of the ground state are suppressed as ϵ is increased from zero to values larger than Δ. We shall come back to this point in Sec. VI.

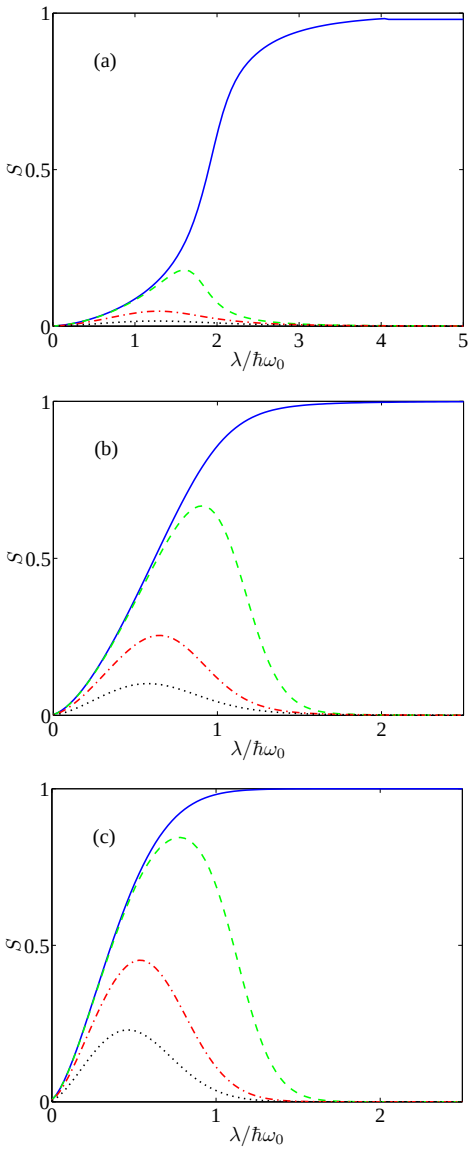

FIG. 10: (Color online) The qubit's entropy S (which quantifies the qubit-oscillator entanglement) in the ground state as a function of $\lambda/(\hbar\omega_0)$. The ratio $\hbar\omega_0/\Delta$ is 0.1 in (a), 1 in (b) and 10 in (c), and the different curves in each panel correspond to $\epsilon/\Delta = 0$ (blue, solid line), 0.1 (green, dashed line), 0.5 (red, dash-dotted line) and 1 (black, dotted line). For $\epsilon = 0$ the qubit-oscillator entanglement increases from zero to one as λ is increased, regardless of the relation between $\hbar\omega_0$ and $E_{\rm q}$. However, the entanglement drops rapidly (especially for large values of λ) as ϵ is increased, i.e. when the qubit is moved away from the degeneracy point.

In Fig. 11 we examine the value of λ at which the qubit's ground-state entropy has the values 0.1 and 0.5. These curves serve as indicators for the onset of qubit-oscillator entanglement, which is related to the instability encountered in the semi-classical calculation. For a high-frequency qubit, the sharp rise in entanglement oc-

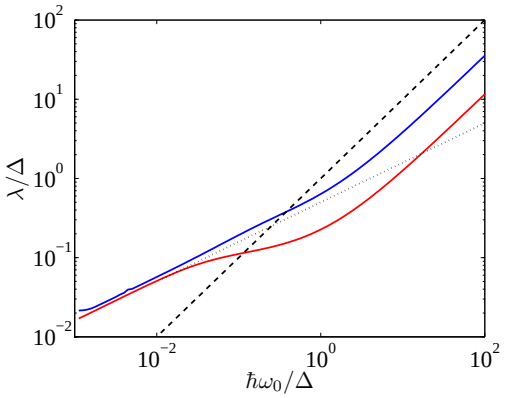

FIG. 11: (Color online) The value of λ/Δ at which the qubit's ground-state entropy has the values 0.1 (red, lower solid line) and 0.5 (blue, upper solid line) plotted as a function of $\hbar\omega_0/\Delta$ (Note the logarithmic scale). Here we take $\epsilon = 0$. The straight lines are given by the formulae $\lambda = \sqrt{\hbar\omega_0 E_q}/2$ (dotted line) and $\lambda = \hbar\omega_0$ (dashed line), which we have obtained in Sec. III. For small values of $\hbar\omega_0/\Delta$, the onset of entanglement occurs when $\lambda = \sqrt{\hbar\omega_0 E_q}/2$. For large values of $\hbar\omega_0/\Delta$, the onset of entanglement occurs when $\lambda \sim \hbar\omega_0$, in agreement with the dependence explained in Sec. III.

curs at $\lambda = \sqrt{\hbar\omega_0 E_q}/2$ which agrees with the instability condition of Secs. III C and III D. For a high-frequency oscillator, the entanglement rises to large values when $\lambda \sim \hbar\omega_0$, in agreement with the analysis of Sec. III B.

V. PREPARATION AND DETECTION OF NONCLASSICAL STATES THROUGH *IN-SITU* PARAMETER AND STATE MANIPULATION

We have seen in Sec. IV that oscillator squeezed states and qubit-oscillator entangled states can occur naturally as ground states of the strongly coupled system. Schrödinger-cat states in the oscillator, i.e. not involving entanglement with the qubit, do not occur as ground states of this system.

One method that has been proposed for the generation of oscillator Schrödinger-cat states in the context of cavity QED [2] can be considered here as well: One prepares a qubit-oscillator entangled state of the form

$$\frac{1}{\sqrt{2}}\left(|\alpha\rangle \otimes |q_1\rangle + |-\alpha\rangle \otimes |q_2\rangle\right), \tag{35}$$

with $|q_1\rangle$ and $|q_2\rangle$ being any two orthogonal qubit states and $|\pm\alpha\rangle$ being coherent states of the oscillator with a large value of $|\alpha|$. One now measures the qubit in the $(|q_1\rangle \pm |q_2\rangle)/\sqrt{2}$ basis. Depending on the outcome of the measurement, the state of the oscillator is projected into one of the two states

$$\frac{1}{\sqrt{2}}\left(|\alpha\rangle \pm |-\alpha\rangle\right), \tag{36}$$

each of which is a Schrödinger-cat state. Since the ground state well above the critical point is approximately given by

$$\frac{1}{\sqrt{2}}\left(|\alpha\rangle \otimes |\downarrow\rangle + |-\alpha\rangle \otimes |\uparrow\rangle\right), \tag{37}$$

with $\alpha = x_0$, the above procedure could also be implemented in the system under consideration (We shall also give an alternative procedure below). Hence all three types of nonclassical states that we consider in this paper can be generated in principle.

One important question that arises in the case of strong qubit-oscillator coupling is whether it is possible to detect the nonclassical states in spite of the always-present strong coupling. The answer is yes, in principle. An important point to note in this context is that, as shown in Secs. III and IV, the energy eigenstates of the system are approximately product states when the qubit is biased far from the degeneracy point, i.e. for large values of ϵ. One could therefore say that, for certain procedures, the qubit and oscillator can be made to effectively decouple from each other by biasing the qubit away from the degeneracy point.

We now discuss some possible procedures for the experimental observation of the different nonclassical states. Since all three types of nonclassical states occur in the case of a high-frequency, adiabatically adjusting qubit, we focus on this case. An experiment could start by preparing the ground state with the qubit biased at the degeneracy point. Under suitable conditions, this step could be achieved by biasing the qubit at the degeneracy point and letting the system relax to its ground state. The state would then be either a squeezed state or an entangled state, depending on the coupling strength. One could then move the qubit away from the degeneracy point for measurement purposes. If the change is slow on the timescales of both the qubit and the oscillator, the system will remain close to its ground state, adiabatically following the bias-point shift (There might be substantial excitation out of the ground state in the double-well regime where the separation between the lowest energy levels is small; however, this situation will come to an end when the double-well potential transforms into a single-well potential). If the system follows its instantaneous ground state during the bias-point sweep, the nonclassical state will be lost. The sweep therefore has to be fast at least compared to the period of the oscillator. If the sweep is adiabatic with respect to the qubit but fast with respect to the oscillator, the qubit will follow the change adiabatically, while the oscillator will be frozen in its initial state. In the case where the initial ground state is a squeezed state, one would achieve the effective qubit-oscillator decoupling while preserving the squeezed state for the measurement step of the experiment. In the case where the initial ground state is (approximately) the entangled state given in Eq. (37), the qubit will end up in its ground state at the final bias point, and this state will be independent of the state of the oscillator. As a

result, the oscillator is left in a Schrödinger-cat state. If the bias-point sweep is fast on both the qubit and oscillator timescales, both subsystems will be frozen in their initial state during the sweep, such that one ends up with an entangled state at the end of the sweep.

The state of the oscillator can be reconstructed using Wigner tomography, which could be implemented following the experiment in Ref. [21]. In that experiment, the oscillator was put into resonance with a qubit that was initialized in its ground state, and the excitation probability of the qubit as a function of time was determined by performing an ensemble of measurements. By decomposing the signal into its Fourier components, it was possible to extract the occupation probabilities of the different photon-number states. When combined with the ability to shift the oscillator's state (through the application of a classical driving signal) before the measurement, full Wigner tomography becomes possible. In the case of a low-frequency oscillator, the transfer of excitations between the qubit and the oscillator can be induced by driving the red or blue sideband, as was done in the experiment of Ref. [3]. Since, as explained above, the qubit is effectively decoupled from the resonator when $\epsilon \gg \Delta$, the exchange of excitations between the qubit and the oscillator would not be efficient at the measurement bias point, which seems to pose a dilemma for the proposed experiment. This difficulty can be circumvented, however, by using a second, weakly coupled qubit for measurement purposes.

Wigner tomography can be used to demonstrate squeezed and Schrödinger-cat states in the oscillator. Qubit-oscillator entangled states could be demonstrated by measuring the correlation between the states of the qubit and oscillator. Starting from the ground state, if the qubit is measured and found to be in the state $|\uparrow\rangle$, the oscillator must be in the state $|-\alpha\rangle$, with $\alpha = x_0$. If the qubit is found to be in the state $|\downarrow\rangle$, the oscillator must be in the state $|\alpha\rangle$. The observation of only these correlations, however, is not sufficient in order to establish the presence of quantum correlations. For that purpose one has to perform measurements in more than one set of bases. The additional qubit basis can be $(|\uparrow\rangle \pm |\downarrow\rangle)/\sqrt{2}$: If the qubit is found to be in the state $(|\uparrow\rangle + |\downarrow\rangle)/\sqrt{2}$, the oscillator must be in the state $(|\alpha\rangle + |-\alpha\rangle)/\sqrt{2}$, and a similar relation holds for the minus signs. The two states $(|\alpha\rangle \pm |-\alpha\rangle)/\sqrt{2}$ can be distinguished through the fact that the state with the plus sign contains only even photon numbers while the state with the minus sign contains only odd photon numbers.

Finally it should be noted that after the bias-point sweep, the resulting state would not be a stationary state and would therefore have a time dependence. This time dependence has to be taken into account in the measurement sequence. Furthermore, when the qubit is biased such that it is in one of the two $\hat{\sigma}_z$ eigenstates, say $|\uparrow\rangle$, the effective oscillator potential will be shifted from the point $x = 0$, and one must take into account this shift when analyzing the post-sweep dynamics.

VI. DECOHERENCE

We now turn to the question of how coupling to the environment affects the prospects of preparing and observing nonclassical states in the system under consideration. Following a standard procedure [28, 32, 33], we analyze the effects of the environment by first determining the energy eigenstates of the system in isolation and then analyzing the relaxation and dephasing rates that govern the decoherence between the different energy eigenstates. For our purposes it will be sufficient to consider Markovian decoherence dynamics.

Since the preparation of nonclassical states above required biasing the system at the point $\epsilon = 0$, we focus on this case. In Secs. III and IV, we found two types of low-lying energy eigenstates, depending on the coupling strength. For small values of λ, where the ground state involves a squeezed state of the oscillator, the energy eigenstates are slightly modified from the energy eigenstates in the absence of qubit-oscillator coupling. For large values of λ, the low-lying energy eigenstates are superpositions similar to that given in Eq. (37). As we shall see below, there is a qualitative difference in how these two types of states are affected by the environment.

The relaxation rate $\Gamma_{i\to j}$ and the dephasing rate $\Gamma_{\varphi,ij}$ involving states i and j are given by [28, 32]

$$\begin{aligned} \Gamma_{i\to j} &= \frac{\pi}{2} S\left(\frac{E_i - E_j}{\hbar}\right) \times \left|\langle i|\, \hat{A}\, |j\rangle\right|^2 \\ \Gamma_{\varphi,ij} &= \pi S(0) \times \left|\langle i|\, \hat{A}\, |i\rangle - \langle j|\, \hat{A}\, |j\rangle\right|^2, \end{aligned} \tag{38}$$

where $S(\omega)$ is the environment's spectral density of the relevant environment operator at frequency ω, and $\hat{A}$ is the system operator through which the system couples to the environment.

In order to go further with the analysis, we need to specify the operator $\hat{A}$ that describes the coupling to the environment; there is one such operator for each decoherence channel. It was mentioned in the introduction that the availability of the tuning parameter ϵ can be seen as an advantage of solid-state qubits in comparison to natural atoms in cavity QED. On the other hand, however, this property also opens an additional channel for noise and the environment to couple to the system. The operator associated with the parameter ϵ is $\hat{\sigma}_z$, and the coupling through this operator is typically the most detrimental for superconducting qubit circuits. We therefore start by considering this decoherence channel.

For coupling through the operator $\hat{\sigma}_z$, the relaxation and dephasing rates are proportional to the quantities $|\langle i|\, \hat{\sigma}_z\, |j\rangle|^2$ and $|\langle i|\, \hat{\sigma}_z\, |i\rangle - \langle j|\, \hat{\sigma}_z\, |j\rangle|^2$, respectively. For $\epsilon = 0$ and small λ (and avoiding the resonant case), the energy eigenstates are approximately product states with the qubit being in an eigenstate of $\hat{\sigma}_x$, to which we refer as $|\pm\rangle$, and the oscillator having a certain number of photons n. The above quantities are then approximately

given by the corresponding values for the qubit states:

$$\begin{aligned}\langle n,+|\,\hat{\sigma}_z\,|n',-\rangle &= \delta_{n,n'}\\ \langle n,+|\,\hat{\sigma}_z\,|n',+\rangle &= \langle n,-|\,\hat{\sigma}_z\,|n',-\rangle = 0. \end{aligned} \quad (39)$$

These expressions suggest that the system relaxes with a rate equal to that of the isolated qubit. The vanishing of the dephasing rate in this approximation has the same origin as its vanishing for an isolated qubit at the degeneracy point, namely the fact that the energies are insensitive to variations in ϵ to first order. This property points out an important requirement for the above expressions to be valid: the energy-level separation must be much larger than the transverse fluctuations in the Hamiltonian. These fluctuations, which are transverse at the degeneracy point, are responsible for dephasing away from the degeneracy point. As a result, in order to obtain the degeneracy-point protection from dephasing, the energy-level separation must be large compared to the dephasing rate when the latter is calculated away from the degeneracy point:

$$\begin{aligned}\Gamma_{\varphi,ij} &= \pi S(0)\times\left|\langle n,\uparrow|\,\hat{\sigma}_z\,|n,\uparrow\rangle - \langle n',\downarrow|\,\hat{\sigma}_z\,|n',\downarrow\rangle\right|^2\\ &= 4\pi S(0). \end{aligned} \quad (40)$$

This parameter is typically of the order of 100 MHz, which corresponds to a dephasing time of 10 ns. At the degeneracy point, an isolated qubit is protected from this noise because the qubit's gap is typically larger than 1 GHz, and the qubit-environment coupling is transverse to the qubit Hamiltonian. Similarly, mildly squeezed states (whose energy-level separations are comparable to those of the simple product states of the uncoupled system) should be protected from dephasing caused by the weak, transverse coupling to the environment. The situation is quite different for large values of λ, where the low-lying states are highly entangled states with a very small separation within an energy-level pair. For example, when $\epsilon = 0$, the lowest two energy eigenstates are given by

$$\frac{1}{\sqrt{2}}\left(|\alpha\rangle\otimes|\downarrow\rangle \pm |-\alpha\rangle\otimes|\uparrow\rangle\right), \quad (41)$$

with $\alpha = x_0$. The energy separation between these states can be obtained from the WKB calculation of Sec. III C. When ϵ exceeds this (possibly very small) energy separation, the energy eigenstates are simply the product states $|\alpha\rangle\otimes|\downarrow\rangle$ and $|-\alpha\rangle\otimes|\uparrow\rangle$. In order for the entangled states to be robust against fluctuations in ϵ, their energy-level separation (at $\epsilon = 0$) must be much larger than the qubit's dephasing rate of about 100 MHz. Since the qubit and oscillator frequencies can be of the order of 1 GHz, one could obtain an entangled ground state that is separated from the first excited state by 100 MHz or more. For example, taking $\lambda = \hbar\omega_0 = \Delta = 1$ GHz, we obtain a qubit ground-state entropy of 0.85 and an energy separation of 138 MHz. However, it would be highly desirable to reduce the qubit decoherence rates, and in principle this should be possible in the future using better materials and circuit designs.

Even though superconducting harmonic oscillators generally have much higher quality factors than superconducting qubits, it is instructive to briefly discuss the effect of oscillator decoherence. The oscillator typically couples to its environment through the same operator that describes its coupling to the qubit. In the present problem, this operator is $\hat{x}$, or equivalently $\hat{a}+\hat{a}^\dagger$. In a free oscillator, the relevant matrix element for purposes of determining the decoherence rates is given by

$$\langle n|\left(\hat{a}+\hat{a}^\dagger\right)|n'\rangle = \sqrt{n}\delta_{n-1,n'} + \sqrt{n+1}\delta_{n+1,n'}. \quad (42)$$

Using the relations for the relaxation and dephasing rates in Eq. (38), one finds that at low temperatures the effect of the environment is to cause decay to the ground state through the loss of photons; photons are lost one by one, with a rate that is proportional to the photon number (Note that since $\langle n|\left(\hat{a}+\hat{a}^\dagger\right)|n\rangle = 0$, no pure dephasing occurs in this system). The photon-loss process is described by the jump operator $\hat{a}$. In the strongly coupled qubit-oscillator system with the double-well effective potential, the effect of the environment will be drastically different from the simple photon-loss dynamics. Since the effective potential near each one of the local minima has the same shape as the free-oscillator potential, the energy eigenstates $|n,\pm\rangle$ will be entangled states where the qubit is either in the state $|\uparrow\rangle$ or $|\downarrow\rangle$, correlated with an oscillator wave function that is given simply by the free-oscillator state $|n\rangle$ shifted to the left or right by a distance x_0. One therefore finds the matrix elements

$$\begin{aligned}\langle n,\pm|\left(\hat{a}+\hat{a}^\dagger\right)|n',\pm\rangle &= \sqrt{n}\delta_{n-1,n'} + \sqrt{n+1}\delta_{n+1,n'}\\ \langle n,+|\left(\hat{a}+\hat{a}^\dagger\right)|n',-\rangle &= 0. \end{aligned} \quad (43)$$

The fact that the matrix elements in the first line coincide with those of the free oscillator implies that the relaxation rate will be equal to the free-oscillator relaxation rate. Note that this process is no longer described by the jump operator $\hat{a}$, but rather by a properly shifted annihilation operator, $\hat{a} \pm \sqrt{m\omega_0/(2\hbar)}x_0$, depending on whether one is dealing with the left or right well in the effective double-well potential. The relaxation process does not change the state of the qubit, or any superposition involving the left and right wells. Even though the relation

$$\langle n,\pm|\left(\hat{a}+\hat{a}^\dagger\right)|n,\pm\rangle = 0 \quad (44)$$

would suggest that no dephasing should occur between the different energy eigenstates, the alternative basis with localized states $\{|n,\uparrow\rangle, |n,\downarrow\rangle$ gives

$$\left|\langle n,\uparrow|\left(\hat{a}+\hat{a}^\dagger\right)|n,\uparrow\rangle - \langle n,\downarrow|\left(\hat{a}+\hat{a}^\dagger\right)|n,\downarrow\rangle\right|^2 = \frac{8m\omega_0}{\hbar}x_0^2. \quad (45)$$

This result implies that the coupling to the environment will cause dephasing in any quantum superposition involving the two wells, with a tendency to localize the wave function in one of the wells. The rate of this process will be proportional to the product of

the environment's power spectrum at zero frequency and the combination of matrix elements given above. This last quantity is proportional to x_0^2, and it grows indefinitely with increasing coupling strength. If we assume that the power spectrum at zero frequency is comparable to that at the oscillator frequency, the dephasing rate can be much larger than the decay rate of the free oscillator because of the largeness of the quantity $\left|\langle n,\uparrow|\left(\hat{a}+\hat{a}^\dagger\right)|n,\uparrow\rangle - \langle n,\downarrow|\left(\hat{a}+\hat{a}^\dagger\right)|n,\downarrow\rangle\right|^2$. For example taking the oscillator's decay rate to be 0.1-1 MHz and considering states where $\hat{a}$ and $\hat{a}^\dagger$ are of typical size $\sqrt{5}$ (i.e. about five virtual photons in the ground state), we find that the dephasing rate can be of the order of 10-100 MHz, which is comparable to the $\hat{\sigma}_z$-mediated dephasing rate.

We finally discuss the question of temperature. We have considered the possibility of preparing nonclassical states by letting the system cool down to its ground state. One must therefore make sure that the energy-level separation between the ground state and the first excited state is larger than the ambient temperature. In superconducting circuits, the temperature is typically around 20 mK, which can be converted to roughly 1 GHz in frequency units. The ground state must be separated from the excited states by at least that amount in order to achieve high-fidelity preparation of the ground state. Typical qubit and oscillator frequencies are in the few-gigahertz range, not much higher than typical temperatures. Squeezed ground states in the oscillator should be separated from the excited states by an energy comparable to the one present in the uncoupled system, implying that the preparation of these states should be possible. The entangled ground states that occur for strong coupling, however, are separated from the first excited states by energy gaps that decrease rapidly with increasing qubit-oscillator coupling strength. If this energy gap becomes smaller than the 1 GHz temperature level, one would not be able to prepare the entangled ground state simply by letting the system cool down to such a state. However, one could let the system cool down to its ground state away from the degeneracy point and then adiabatically shift the bias point to one with an entangled ground state. Provided that the thermalization rate is sufficiently low, it is not necessary to have a degeneracy-point energy-level separation that is larger than the temperature. The 1 GHz temperature level should therefore not be seen as a fundamental obstacle to the preparation of entangled ground states.

VII. CONCLUSION

We have analyzed the properties of a strongly coupled qubit-oscillator system, focusing on the potential of this system for the preparation of nonclassical states. These states include squeezed states and Schrödinger-cat states of the oscillator, as well as qubit-oscillator entangled states.

We have compared the predictions of four different analytical approaches: the weak-coupling approximation, the adiabatically-adjusting-oscillator approximation, the adiabatically-adjusting-qubit approximation and the semiclassical calculation. Each one of these four approaches is well suited for analyzing the behaviour of the system under a certain set of assumptions. Thus the combination of the results provides a rather thorough understanding of the qubit-oscillator system in the regime of ultrastrong coupling. We have also presented results of numerical calculations that reinforce the results of the analytical derivations. These results demonstrate the nonclassical properties of the energy eigenstates, and especially the ground state, of the system.

We have discussed various possible experimental procedures for the preparation and observation of nonclassical states. All three types of nonclassical states that we discuss in this paper can be prepared and detected in principle.

We have also analyzed the effect of coupling to the environment on the system. We have shown that the decoherence dynamics of the coupled qubit-oscillator system can be qualitatively different from the decoherence dynamics of the qubit or oscillator in isolation. We have shown that nonclassical states, particularly highly-entangled states, are highly susceptible to changes or fluctuations in the bias parameters. These results lead to the conclusion that high degrees of control and low noise levels will be required for the preparation of robust nonclassical states in the ultrastrong-coupling regime.

We would like to thank P. Forn-Diaz, J. R. Johansson, N. Lambert and S. Shevchenko for useful discussions. This work was supported in part by the National Security Agency (NSA), the Army Research Office (ARO), the Laboratory for Physical Sciences (LPS) and the National Science Foundation (NSF) grant No. 0726909.

Note added in proof: Recently ultrastrong coupling between a superconducting flux qubit and a coplanar waveguide resonator has been demonstrated [34].

Appendix A: Oscillator's effective kinetic energy in the case of a high-frequency qubit

In this appendix we briefly discuss the modification to the oscillator's kinetic energy in the case of a high-frequency qubit (see Sec. III C). One could perform the calculation by considering only the kinetic-energy term, without considering the specific form of the trapping potential, i.e. by using the completely delocalized momentum eigenstates as a basis for the calculation. Such a calculation, however, turns out not to lead to simple, transparent results. We therefore consider the corrections that one would need to add to the kinetic-energy term in the effective oscillator Hamiltonian starting from the eigenstates of the free-oscillator Hamiltonian.

The eigenstates of the Hamiltonian $\hat{H}_{\rm ho}$ can be expressed in the position basis as

$$|k\rangle = \int dx \psi_k(x)\,|x\rangle\,. \tag{46}$$

Taking into account the high-frequency, adiabatically adjusting qubit, and for definiteness taking the case of the qubit's ground state, the above eigenstates are modified as follows:

$$\begin{aligned}\left|\tilde{k}\right\rangle &= \int dx\psi_k(x)\left|x\right\rangle\otimes\left|g(x)\right\rangle \\ &= \int dx\psi_k(x)\sum_{k'}\psi^*_{k'}(x)\left|k'\right\rangle\otimes\left|g(x)\right\rangle, \quad (47)\end{aligned}$$

where $|g(x)\rangle$ has the same meaning as $|g_x\rangle$ from Sec. III C. One can now obtain the correction to the kinetic-energy term as:

$$\left\langle\tilde{k}\right|\frac{\hat{p}^2}{2m}\left|\tilde{l}\right\rangle - \langle k|\frac{\hat{p}^2}{2m}|l\rangle = \iint dx_1dx_2\sum_{k'l'}\psi^*_k(x_1)\psi_{k'}(x_1)$$
$$\psi^*_{l'}(x_2)\psi_l(x_2)\langle k'|\frac{\hat{p}^2}{2m}|l'\rangle\left(\langle g(x_1)|\,g(x_2)\rangle - 1\right). (48)$$

The factor between parentheses represents the relative correction to the kinetic-energy term in the Hamiltonian. This factor can be estimated as:

$$\begin{aligned}\langle g(x_1)|\,g(x_2)\rangle - 1 &= \cos\left(\frac{\varphi(x_1)-\varphi(x_2)}{2}\right)-1 \\ &\approx -\frac{[\varphi(x_1)-\varphi(x_2)]^2}{8} \\ &\sim \left(\frac{g(x_1-x_2)}{E_{\rm q}}\right)^2 \\ &\sim \frac{\hbar g^2}{m\omega_0 E_{\rm q}^2}. \quad (49)\end{aligned}$$

In deriving this expression we have taken the case $\epsilon/\Delta \ll 1$ (for which the relative correction is maximum) and taken x to be of the order of the characteristic oscillator length. By comparing the above expression to the relative correction in the potential-energy term found in Sec. III C, i.e. $g^2/(m\omega_0^2 E_{\rm q})$, one can see that the kinetic-term correction is negligible when $\hbar\omega_0 \ll E_{\rm q}$.

[1] E. T. Jaynes and F. W. Cummings, Proc. IEEE **51**, 89 (1963).

[2] See e.g. C. C. Gerry and P. L. Knight, *Introductory Quantum Optics* (Cambridge University Press, 2005); D. F. Walls and G. J. Milburn, *Quantum Optics* (Springer, Berlin, 1994); M. O. Scully and M. S. Zubairy, *Quantum Optics* (Cambridge University Press, 1997).

[3] I. Chiorescu, P. Bertet, K. Semba, Y. Nakamura, C. J. P. M. Harmans, J. E. Mooij, Nature **431**, 159 (2004).

[4] A. Wallraff, D. I. Schuster, A. Blais, L. Frunzio, R.-S. Huang, J. Majer, S. Kumar, S. M. Girvin, R. J. Schoelkopf, Nature **431**, 162 (2004).

[5] For recent reviews on superconducting qubit circuits, see e.g. J. Q. You and F. Nori, Phys. Today **58** (11), 42 (2005); G. Wendin and V. Shumeiko, in *Handbook of Theoretical and Computational Nanotechnology*, ed. M. Rieth and W. Schommers (ASP, Los Angeles, 2006); R. J. Schoelkopf and S. M. Girvin, Nature, **451**, 664 (2008); J. Clarke and F. K. Wilhelm, Nature **453**, 1031 (2008).

[6] K. Hennessy, A. Badolato, M. Winger, D. Gerace, M. Atatüre, S. Gulde, S. Fält, E. L. Hu, and A. Imamoglu, Nature (London) **445**, 896 (2007).

[7] R. Leturcq, C. Stampfer, K. Inderbitzin, L. Durrer, C. Hierold, E. Mariani, M. G. Schultz, F. von Oppen, and K. Ensslin, Nat. Phys. **5**, 327 (2009); M. D. LaHaye, J. Suh, P. M. Echternach, K. C. Schwab, and M. L. Roukes, Nature **459**, 960 (2009); G. A. Steele, A. K. Hüttel, B. Witkamp, M. Poot, H. B. Meerwaldt, L. P. Kouwenhoven, and H. S. J. van der Zant, Science **325**, 1103 (2009).

[8] A. D. Armour, M. P. Blencowe, and K. C. Schwab, Phys. Rev. Lett. **88**, 148301 (2002).

[9] T. Holstein, Ann. Phys. (N.Y.) **8**, 325 (1959).

[10] See e.g. R. Graham and M. Höhnerbach, Z. Phys **57**, 233 (1984); L. Müller, J. Stolze, H. Leschke, and P. Nagel, Phys. Rev. A **44**, 1022 (1991).

[11] H. J. Kimble, Phys. Scr. **T76**, 127 (1998); J. M. Raimond, M. Brune, and S. and Haroche, Rev. Mod. Phys. **73**, 565 (2001); S. Haroche and J. M. Raimond, *Exploring the Quantum: Atoms, Cavities, and Photons* (Oxford University Press, 2006).

[12] M. H. Devoret. S. Girvin and R. Schoelkopf, Ann. Phys. **16**, 767 (2007).

[13] A. P. Hines, C. M. Dawson, R. H. McKenzie, and G. J. Milburn, Phys. Rev. A **70**, 022303 (2004).

[14] E. K. Irish, J. Gea-Banacloche, I. Martin, and K. C. Schwab, Phys. Rev. B **72**, 195410 (2005); E. K. Irish, Phys. Rev. Lett. **99**, 173601 (2007).

[15] J. Larson, Phys. Scr. **76**, 146 (2007); Phys. Rev. A **78**, 033833 (2008); arXiv:0908.1717.

[16] D. Zueco, G. M. Reuther, S. Kohler, and P. Hänggi, Phys. Rev. A **80**, 033846 (2009).

[17] C. P. Meaney, T. Duty, R. H. McKenzie, and G. J. Milburn, arXiv:0903.2681.

[18] I. Lizuain, J. Casanova, J. J. Garcia-Ripoll, J. G. Muga, and E. Solano, arXiv:0912.3485.

[19] See e.g. W. D. Oliver, Y. Yu, J. C. Lee, K. K. Berggren, L. S. Levitov, T. P. Orlando, Science **310**, 1653 (2005); D. M. Berns, W. D. Oliver, S. O. Valenzuela, A. V. Shytov, K. K. Berggren, L. S. Levitov, and T. P. Orlando, Phys. Rev. Lett. **97**, 150502 (2006).

[20] See e.g. F. G. Paauw, A. Fedorov, C. J. P. M. Harmans, and J. E. Mooij, Phys. Rev. Lett. **102**, 090501 (2009).

[21] M. Hofheinz, E. M. Weig, M. Ansmann, R. C. Bialczak, E. Lucero, M. Neeley, A. D. O'Connell, H. Wang, J. M. Martinis, and A. N. Cleland, Nature **454**, 310 (2008); M. Hofheinz, H. Wang, M. Ansmann, R. C. Bialczak, E. Lucero, M. Neeley, A. D. O'Connell, D. Sank, J. Wenner, J. M. Martinis and A. N. Cleland, Nature **459**, 546 (2009).

[22] See also A. A. Houck, D. I. Schuster, J. M. Gambetta, J. A. Schreier, B. R. Johnson, J. M. Chow, L. Frunzio, J. Majer, M. H. Devoret, S. M. Girvin, and R. J. Schoelkopf, Nature **449**, 328 (2007); M. A. Sillanpää, J. I. Park, and

R.W. Simmonds, Nature **449**, 438 (2007).

[23] For recent proposals for the generation of squeezed and Schrödinger-cat states in superconducting resonators, see e.g. Y.-X. Liu, L.-F. Wei, and F. Nori, Europhys. Lett. **67**, 941 (2004); Phys. Rev. A **71**, 063820 (2005); M. Mariantoni, F. Deppe, A. Marx, R. Gross, F. K. Wilhelm, and E. Solano, Phys. Rev. B **78**, 104508 (2008); A. M. Zagoskin, E. Ilichev, M. W. McCutcheon, J. F. Young, and F. Nori, Phys. Rev. Lett. **101**, 253602 (2008); M. Abdel-Aty, Opt. Commun. **282**, 4556 (2009); J. R. Johansson, G. Johansson, C. M. Wilson, and F. Nori, Phys. Rev. Lett. **103**, 147003 (2009).

[24] J. Bourassa, J. M. Gambetta, A. A. Abdumalikov, O. Astafiev, Y. Nakamura, and A. Blais, Phys. Rev. A **80**, 032109 (2009).

[25] B. Peropadre, P. Forn-Diaz, E. Solano, and J. J. Garcia-Ripoll, arXiv:0912.3456.

[26] See e.g. S. N. Shevchenko, S. Ashhab, and F. Nori, Phys. Rep. (in press).

[27] M. A. Sillanpää, T. Lehtinen, A. Paila, Yu. Makhlin, L. Roschier, and P. J. Hakonen, Phys. Rev. Lett. **95**, 206806 (2005); T. Duty, G. Johansson, K. Bladh, D. Gunnarsson, C. Wilson, and P. Delsing, Phys. Rev. Lett. **95**, 206807 (2005); G. Johansson, L. Tornberg, and C. M.Wilson, Phys. Rev. B **74**, 100504(R) (2006); V. I. Shnyrkov, Th. Wagner, D. Born, S. N. Shevchenko, W. Krech, A. N. Omelyanchouk, E. Ilichev, and H.-G. Meyer, Phys. Rev. B **73**, 024506 (2006); S. N. Shevchenko, S. H. W. van der Ploeg, M. Grajcar, E. Il'ichev, A. N. Omelyanchouk, H.-G. Meyer, Phys. Rev. B **78**, 174527 (2008).

[28] See e.g. C. Cohen-Tannoudji, J. Dupont-Roc, and G. Grynberg, *Atom-Photon Interactions* (Wiley, New York, 1992).

[29] An explanation of Van Vleck perturbation theory can be found in J. Hausinger and M. Grifoni, New J. Phys. **10**, 115015 (2008); An application to superconducting-qubit circuits with high-frequency couplers is given in S. Ashhab, A. O. Niskanen, K. Harrabi, Y. Nakamura, T. Picot, P. C. de Groot, C. J. P. M. Harmans, J. E. Mooij, and F. Nori, Phys. Rev. B **77**, 014510 (2008).

[30] R. H. Dicke, Phys. Rev. **93**, 99 (1954).

[31] K. Hepp and E. H. Lieb, Ann. Phys. **76**, 360 (1973); Y. K. Wang and F. T. Hioe, Phys. Rev. A **7**, 831 (1973); See also N. Lambert, C. Emary, and T. Brandes, Phys. Rev. Lett. **92**, 073602 (2004); P. Nataf and C. Ciuti, Phys. Rev. Lett. **104**, 023601 (2010).

[32] G. Ithier, E. Collin, P. Joyez, P. J. Meeson, D. Vion, D. Esteve, F. Chiarello, A. Shnirman, Y. Makhlin, J. Schriefl, and G. Schön, Phys. Rev. B **72**, 134519 (2005).

[33] For a recent study on a related problem, see e.g. S. De Liberato, D. Gerace, I. Carusotto, and C. Ciuti, Phys. Rev. A **80**, 053810 (2009).

[34] T. Niemczyk, F. Deppe, H. Huebl, E. P. Menzel, F. Hocke, M. J. Schwarz, J. J. Garcia-Ripoll, D. Zueco, T. Hümmer, E. Solano, A. Marx, and R. Gross, arXiv:1003.2376v1.